

Entanglement-assisted capacity regions and protocol designs for quantum multiple-access channels

Haowei Shi,¹ Min-Hsiu Hsieh,² Saikat Guha,¹ Zheshen Zhang,^{1,3} and Quntao Zhuang^{1,4,*}

¹*James C. Wyant College of Optical Sciences, University of Arizona, Tucson, Arizona 85721, USA*

²*Hon Hai Research Institute, Taipei, 114, Taiwan*

³*Department of Materials Science and Engineering,
University of Arizona, Tucson, Arizona 85721, USA*

⁴*Department of Electrical and Computer Engineering,
University of Arizona, Tucson, Arizona 85721, USA*

We solve the entanglement-assisted (EA) classical capacity region of quantum multiple-access channels with an arbitrary number of senders. As an example, we consider the bosonic thermal-loss multiple-access channel and solve the one-shot capacity region enabled by an entanglement source composed of sender-receiver pairwise two-mode squeezed vacuum states. The EA capacity region is strictly larger than the capacity region without entanglement-assistance. With two-mode squeezed vacuum states as the source and phase modulation as the encoding, we also design practical receiver protocols to realize the entanglement advantages. Four practical receiver designs, based on optical parametric amplifiers, are given and analyzed. In the parameter region of a large noise background, the receivers can enable a simultaneous rate advantage of 82.0% for each sender. Due to teleportation and superdense coding, our results for EA classical communication can be directly extended to EA quantum communication at half of the rates. Our work provides a unique and practical network communication scenario where entanglement can be beneficial.

I. INTRODUCTION

Communication channels model physical media for information transmission. In the case of a single-sender single-receiver channel, the Shannon capacity theorem [1, 2] concludes that a channel is essentially characterized by a single quantity—the channel capacity. As physical media obey quantum physics, the channel model eventually needs to incorporate quantum effects during the transmission, which has re-shaped our understanding of communication. To begin with, the Shannon capacity has been generalized to the Holevo-Schumacher-Westmoreland (HSW) classical capacity [3–5]. Quantum effects such as entanglement have also enabled non-classical phenomena in communication, such as superadditivity [6–11] and capacity-boost from entanglement-assistance (EA) [12–21]. Moreover, reliable transmission of quantum information is possible, established by the Lloyd-Shor-Devetak quantum capacity theorem [22–24]. Combining different types of information transmission, Refs. 25 and 26 provide a capacity formula for the simultaneous trade-off of classical information (bits), quantum information (qubits) and quantum entanglement (ebits).

Despite their exact evaluation being prevented by the superadditivity dilemma, capacities of single-sender single-receiver quantum channels are well-understood. In particular, the benefits of entanglement in boosting the classical communication rates have been known since the pioneering theory works [12–15, 17] and recently experimentally demonstrated [27] in a thermal-loss bosonic communication channel. The two-mode-

squeezed-vacuum (TMSV) state is utilized as the entanglement source and functional quantum receivers are demonstrated, thanks to the practical protocol design in Ref. [28]. Further development of receiver designs [29] and the application to covert communication [30] have also been considered.

However, supported by the Internet, real-life communication scenarios, such as online lectures and online conferences, often involve multiple senders and/or receivers. As a common paradigm being studied in the literature [31–35], the multiple-access channel (MAC) concerns multiple senders and a single receiver. Communication over a MAC is no longer characterized by a single rate, but a rate region with a trade-off between multiple senders. With the development of a quantum network [36–40], quantum effects have also become relevant in such a communication scenario. In this regard, the classical capacity region of a quantum MAC was solved by Winter [41], while the entanglement-assisted (EA) classical communication capacity region in the special case of a two-sender MAC was solved in Ref. [17]. Although superadditivity in the capacity region has also been found in a MAC [42, 43] and EA advantage in a classical MAC can be shown [33], it is unclear how much advantage entanglement can provide for a quantum MAC in a direct communication scenario.

In this work, we present a thorough study of EA classical communication over a quantum MAC with an arbitrary number of senders. On the fundamental information-theoretic side, we prove the general EA classical capacity theorem for an s -sender ($s \geq 2$) MAC, which has been conjectured in Ref. [17] and yet not proven for the past decade. Next, we proceed to evaluate the EA rate region of the bosonic thermal-loss MAC, which models an optical or microwave communication

* zhuangquntao@email.arizona.edu

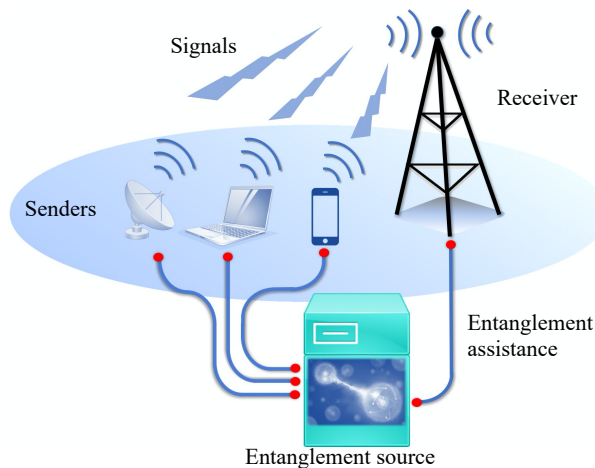


Figure 1. **Conceptual schematic of EA classical communication over a MAC.** The entanglement source distributes entangled pairs to each sender and the receiver, potentially via a quantum network. The senders encode their own message on their share and send the signals to the receiver. The receiver decodes the messages of all senders by jointly measuring the received signal and the entanglement assistance locally stored.

scenario (see Fig. 1), and find rigorous advantages from entanglement. Finally, on the application layer, we propose practical protocols to realize the EA advantage in a bosonic thermal-loss MAC, and provide a variety of transmitter and receiver designs. Due to teleportation [45] and superdense coding [12], our results for EA classical communication can be directly extended to EA quantum communication at half of the rates. As bosonic thermal-loss MACs model various real-world communication networks, our EA communication scenario is widely applicable to radio-frequency, deep-space [46], and wireless communication scenarios [47].

II. RESULTS

In a MAC, multiple senders individually communicate with a single receiver. As shown in Fig. 1, besides a transmitter that sends encoded messages, each sender has access to entanglement pre-shared with the receiver, potentially through a ground-satellite and/or fiber-based quantum network. The receiver decodes all messages from the senders via a joint measurement on all received signals and the stored EA. Our first main result is an EA capacity theorem which quantifies the trade-off between the ultimate communication rates of different senders. The capacity formula has a form of conditional quantum mutual information, analogous to the classical formula [2]. We then give an explicit example of a bosonic thermal-loss MAC and evaluate its rate-region with the common TMSV entanglement source. Comparing it with the case without EA [44], we find great advantages enabled by

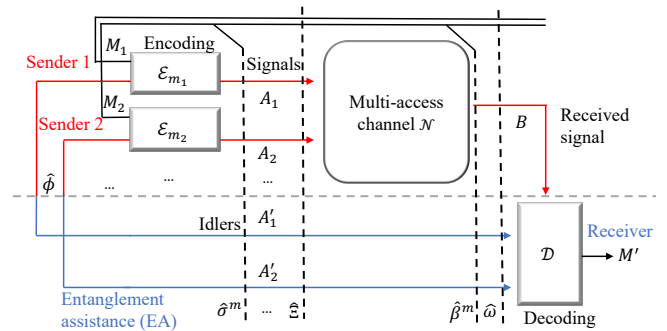


Figure 2. **Schematic of a general EA-MAC communication protocol.** The EA sources $\hat{\phi}$ of the s senders are in a product state of Eq. (1). The s senders apply independent encoding modeled by quantum operations, i.e., sender k applies \mathcal{E}_{m_k} on the signal state given the message m_k . Denoting the entire message as $m = m_1 \cdots m_s$, the encoded signal-idler is then in a state $\hat{\sigma}^m$. The senders' encoded quantum systems $A = A_1 \cdots A_s$ are sent through the MAC \mathcal{N} , leading to the output system B . The receiver applies the quantum operation \mathcal{D} to decode the information from the joint state $\hat{\beta}^m$ of the output system B and the pre-shared reference systems $A' = A'_1 \cdots A'_s$. We define M_k as the codeword space of each message m_k , M as the overall codeword space of message m , and M' as the decoded codeword space. To facilitate the analysis, we denote the overall state $\hat{\Xi}$ (Eq. (A1)) over systems MAA' right before the channel and the overall state $\hat{\omega}$ (Eq. (A2)) over systems MBA' right before the decoding.

entanglement; Moreover, when the sources of all senders have equal and low brightness, we numerically find that the TMSV source is optimal at a corner rate point. As a benchmark, we derive bounds on the capacity region and design practical protocols, based only on off-the-shelf quantum optical elements, which can achieve quantum advantages from entanglement in the near-term.

A. EA classical capacity theorem for MAC

1. Multiple-access channels

As depicted in Fig. 2, consider a MAC with s senders, each sending a message m_k ($1 \leq k \leq s$) sampled from a message space M_k , therefore the overall message $m = m_1 \cdots m_s$ is sampled from the message space $M = \otimes_{k=1}^s M_k$. To send each message m_k , the k th sender performs a quantum operation \mathcal{E}_{m_k} to produce a signal quantum system A_k . Following Ref. [17], we introduce EA in the above communication scenario—namely the receiver has a reference system A'_k (idler) pre-shared with the EA with the k th sender.

We consider the entanglement to be pairwise between each sender and the receiver such that the overall quantum state

$$\hat{\phi}_{AA'} = \otimes_{k=1}^s \hat{\phi}_{A_k A'_k} \quad (1)$$

is in a product form, where we have denoted $A = A_1 \cdots A_s$ and $A' = A'_1 \cdots A'_s$ as the overall systems.

After the encoding, the composite system A containing all of the quantum systems $\{A_k\}_{k=1}^s$ is input to the MAC $\mathcal{N}_{A \rightarrow B}$, which outputs the quantum system B for the receiver to decode the messages jointly with the EA A' . For convenience, we define a quantum state after the channel but without the encoding, $\hat{\rho}_{BA'} = [\mathcal{N}_{A \rightarrow B} \otimes \mathcal{I}] (\hat{\phi}_{AA'})$, where \mathcal{I} is the identity channel modeling the ideal storage of the idler system. The formal analyses of the quantum-state evolution can be found in Appendix A.

The performance metric of the above communication scenario is described by a vector of rates (R_1, \dots, R_s) , where R_k is the reliable communication rate between the k th sender and the receiver (see Appendix A, Section II of Ref. [41], and Subsection III.A of Ref. [17] for the formal definitions). These rates in general have non-trivial trade-offs with each other. In the case without EA, the capacity region is well-established by the pioneering work of Winter [41] (see Appendix C).

To describe the rate region of the s -sender MAC, we will frequently divide the senders into two blocks, the block of interest indexed by a sequence J and the complementary block J^c . For example, when $s = 2$, we have four possible block divisions: $\{J = 1, J^c = 2\}$, $\{J = 2, J^c = 1\}$, and two trivial cases $\{J = 1, 2, J^c = \emptyset\}$, $\{J = \emptyset, J^c = 1, 2\}$. Any s -fold quantity can be written as a composition of the two blocks, e.g., message space $M = M[J]M[J^c]$, with $M[J] = \otimes_{i \in J} M_i$, $M[J^c] = \otimes_{i \in J^c} M_i$; similarly the message as $m = m[J]m[J^c]$.

2. Capacity theorem

To present our EA-MAC capacity theorem for the scenario in Fig. 2, we introduce some entropic quantities. For a quantum system XYZ in a state $\hat{\alpha}$, we define the quantum mutual information between X and Y as

$$I(X : Y)_{\hat{\alpha}} = S(X)_{\hat{\alpha}} + S(Y)_{\hat{\alpha}} - S(XY)_{\hat{\alpha}},$$

where $S(X)_{\hat{\alpha}} = S(\hat{\alpha}_X) = -\text{tr}(\hat{\alpha}_X \log_2 \hat{\alpha}_X)$ is the von Neumann entropy. Similarly, the quantum conditional mutual information between X and Z conditioned on Y

$$I(X; Z|Y)_{\hat{\alpha}} = S(XY)_{\hat{\alpha}} + S(YZ)_{\hat{\alpha}} - S(XYZ)_{\hat{\alpha}} - S(Y)_{\hat{\alpha}}.$$

With the entropic quantities in hand, we can present our main theorem below (see Appendix D for a proof).

Theorem 1 (EA-MAC capacity) *The entanglement-assisted classical communication capacity region over an s -sender MAC \mathcal{N} is given by the regularized union*

$$\mathcal{C}_E(\mathcal{N}) = \overline{\bigcup_{\ell=1}^{\infty} \frac{1}{\ell} \mathcal{C}_E^{(1)}(\mathcal{N}^{\otimes \ell})} \quad (2)$$

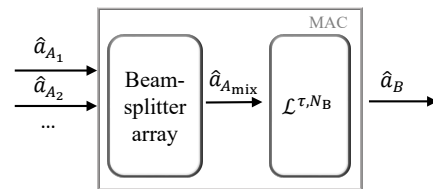


Figure 3. **Schematic of the bosonic thermal-loss MAC.** The beam-splitter array models a linear scattering medium. The thermal-loss channel models the noisy transmission.

where the “one-shot” capacity region $\mathcal{C}_E^{(1)}(\mathcal{N})$ is the convex hull of the union of “one-shot, one-encoding” regions

$$\mathcal{C}_E^{(1)}(\mathcal{N}) = \text{Conv} \left[\bigcup_{\hat{\phi}} \tilde{\mathcal{C}}_E(\mathcal{N}, \hat{\phi}) \right]. \quad (3)$$

The “one-shot, one-encoding” rate region $\tilde{\mathcal{C}}_E(\mathcal{N}, \hat{\phi})$ for the $2s$ -partite pure product state $\hat{\phi}_{AA'} = \otimes_{k=1}^s \hat{\phi}_{A_k A'_k}$ over AA' , is the set of rates (R_1, \dots, R_s) satisfying the following 2^s inequalities

$$\sum_{k \in J} R_k \leq I(A'[J]; B|A'[J^c])_{\hat{\rho}}, \forall J, \quad (4)$$

where the conditional quantum mutual information is evaluated over the output state $\hat{\rho}_{BA'} = \mathcal{N}_{A \rightarrow B} \otimes \mathcal{I}(\hat{\phi}_{AA'})$.

Here we make some remarks about Theorem 1: First, if we only focus on the regularized capacity region $\mathcal{C}_E(\mathcal{N})$, then the convex hull in Eq. (3) is not necessary, as one can simply include the time-sharing over different inputs among the infinite number of channel uses; However, if one wants to formulate the “one-shot” capacity region $\mathcal{C}_E^{(1)}(\mathcal{N})$, then the convex hull is necessary to include potential time-sharing between any codes. Second, the capacity formula in Ref. [17] can be considered as a special case of our theorem, as the regularized case does not need the convex hull in Eq. (3); indeed, at the end of Ref. [17] our theorem is stated as a conjecture.

B. EA capacity region for a bosonic MAC

1. Bosonic thermal-loss multiple-access channels

In an optical or microwave communication scenario, the relevant MAC is a bosonic thermal-loss MAC depicted in Fig. 3. Upon the input modes $\hat{a}_{A_1} \cdots \hat{a}_{A_s}$ from the s senders, the MAC \mathcal{N} first combines the modes through a beam-splitter array to produce a mixture mode

$$\hat{a}_{A_{\text{mix}}} = \sum_{k=1}^s \sqrt{\eta_k} \hat{a}_{A_k}, \quad (5)$$

while all other ports of the beam-splitter array are discarded, here the weights $\{\eta_k\}$ are non-negative and normalized. Then the mixture mode goes through a bosonic

thermal-loss channel \mathcal{L}^{τ, N_B} described by the operator transform

$$\hat{a}_B = \sqrt{\tau}\hat{a}_{A_{\text{mix}}} + \sqrt{1-\tau}\hat{a}_E, \quad (6)$$

where \hat{a}_E denotes the environment mode in a thermal state with a mean photon number $\langle \hat{a}_E^\dagger \hat{a}_E \rangle = N_B/(1-\tau)$. This convention of fixing the mean photon number N_B of the thermal noise mixed into the output mode \hat{a}_B is widely used, e.g., in quantum illumination [48, 49].

In a bosonic MAC, the Hilbert space of the quantum systems is infinite-dimensional—an arbitrary number of photons can occupy a single mode due to the bosonic nature of light. To model a realistic communication scenario, we will consider an energy constraint on the mean photon number (brightness) of the signals modes

$$\langle \hat{a}_{A_k}^\dagger \hat{a}_{A_k} \rangle = N_{S,k}, 1 \leq k \leq s, \quad (7)$$

which is commonly adopted in bosonic communication [28, 44, 50]. Note that in general the energy of different senders can be different.

Without EA, the capacity region of the above bosonic MAC has been considered in Ref. [44] for the two-user case. However, the generalization of the coherent-state rate region therein to the s -sender case is straightforward, leading to a rate region specified by the following 2^s inequalities,

$$\sum_{i \in J} R_i \leq C_{\text{coh}}^J \equiv g \left(\sum_{i \in J} \tau \eta_i N_{S,i} + N_B \right) - g(N_B), \quad (8)$$

where $g(x) = (x+1) \log_2(x+1) - x \log_2(x)$ and J can be chosen arbitrarily. Moreover, a squeezing-based encoding scheme is shown to be advantageous over the coherent-state encoding; however, regardless of the encoding, the rate region is always bounded by the following set of outer bounds

$$R_k \leq g(\tau N_{S,k} + N_B) - g(N_B), 1 \leq k \leq s, \quad (9)$$

which are derived by assuming a super receiver that can reverse the beamsplitter array in the bosonic thermal-loss MAC. A second outer bound can be obtained from energetic considerations, which leads to the same form of Ineq. (8) with J being all users. As these outer bounds represent the upper limit of all encodings without EA, an EA rate region outside the rate region specified by the above outer bounds will demonstrate a strict advantage enabled by entanglement.

2. EA outer bounds

As the exact evaluation of the EA capacity region for the bosonic MAC is challenging, we first focus on outer bounds to obtain some insights. Similar to the case without EA, via reducing to the single-sender EA classical

capacity, one can obtain outer bounds for the EA-MAC classical capacity region (See Appendix A for a proof). Explicitly, we have

$$R_k \leq C_E(N_{S,k}; \mathcal{L}^{\tau, N_B}), 1 \leq k \leq s, \quad (10a)$$

$$\sum_{k=1}^s R_k \leq C_E \left(\sum_{k=1}^s \eta_k N_{S,k}; \mathcal{L}^{\tau, N_B} \right), \quad (10b)$$

where the explicit formula of the EA capacity $C_E(N_S; \mathcal{L}^{\tau, N_B})$ over a bosonic thermal-loss channel \mathcal{L}^{τ, N_B} , with the energy constraint N_S , can be found in Eq. (A5) of Appendix A. These outer bounds provide the upper limit of EA classical communication rates, and apply to arbitrary forms of entanglement source $\hat{\phi}$ and encoding $\{\mathcal{E}_m\}$.

3. Two-mode squeezed vacuum rate region

To obtain an explicit example of bosonic EA-MAC capacity region, we consider the entanglement source in Eq. (1) as a product of TMSV pairs, each with the wavefunction

$$\hat{\phi}_{A_k A'_k}^{\text{TMSV}} = \sum_{n_k=0}^{\infty} \sqrt{\frac{N_{S,k}^{n_k}}{(N_{S,k}+1)^{n_k+1}}} |n_k\rangle_{A_k} |n_k\rangle_{A'_k}, \quad (11)$$

for $1 \leq k \leq s$, where $|n\rangle$ is the number state defined by $\hat{a}^\dagger \hat{a} |n\rangle = n |n\rangle$. In Ref. [28], it has been shown that the TMSV state is optimal for single-sender single-receiver EA classical communication, therefore we expect the TMSV source to be good in the MAC case. Although, due to the complexity from the plurality of the senders, the exact union over the states in Eq. (3) for the EA-MAC classical capacity region is challenging to solve.

We evaluate the ‘‘one-shot, one-encoding’’ rate region $\tilde{\mathcal{C}}_E(\mathcal{N}, \hat{\phi}^{\text{TMSV}})$ in Ineqs. (4) for the TMSV source in Eq. (11). Although the evaluation of each Ineq. (4) is efficient thanks to the Gaussian nature of the state, the number of such inequalities 2^s is exponential and therefore resource-consuming in practice. To showcase the capacity region, we choose $s = 2, 3$, which enable direct visualization as the rate region is two or three dimensional. In comparison, we also compute the classical coherent-state rate region in Ineq. (8) and the classical outer bound, specified jointly by Ineq. (9) and Ineq. (8) with J being all senders. Moreover, we can also compare $\tilde{\mathcal{C}}_E(\mathcal{N}, \hat{\phi}^{\text{TMSV}})$ with the EA outer bound in Ineqs. (10).

Three representative setups of parameters are chosen as examples. To begin with, we consider an intermediate channel noise $N_B = 20$, identical to the case of microwave quantum illumination [48, 51]; Furthermore, a noisy channel with sufficiently large noise $N_B = 10^4$ is noteworthy as it provides a saturated EA advantage [28]; Finally, the long wavelength infrared domain with relatively small noise $N_B = 0.1$ is a relatively uncharted territory for EA communication, nevertheless also relevant for practical application.

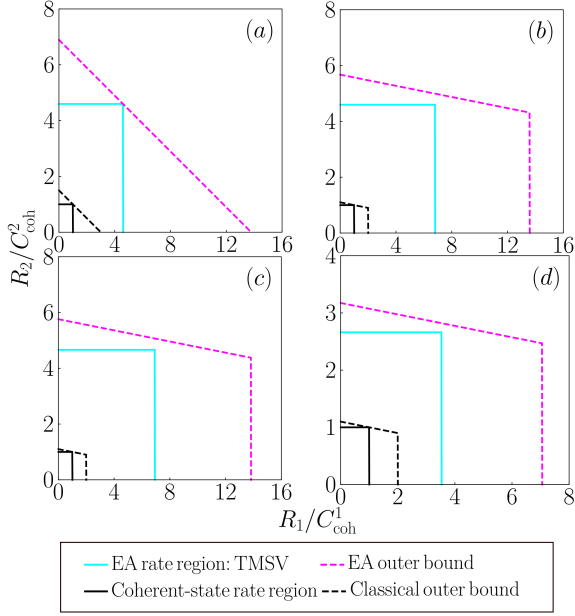


Figure 4. **The symmetric two-sender rate region.** Rates are normalized by the coherent-state bound $C_{\text{coh}}^1, C_{\text{coh}}^2$ defined in Ineq. (8), evaluated in the scenario of (a) microwave domain, $\tau = 0.01, N_B = 20, N_{S,1} = N_{S,2} = 0.01, \eta_1 = 1/3, \eta_2 = 2/3$. (b) microwave domain, $\tau = 0.01, N_B = 20, \eta_1 = \eta_2 = 1/2, N_{S,1} = 0.001, N_{S,2} = 0.01$. (c) a noisy channel, $\tau = 10^{-3}, N_B = 10^4, \eta_1 = \eta_2 = 1/2, N_{S,1} = 0.001, N_{S,2} = 0.01$. (d) long wavelength infrared domain $\eta_1 = \eta_2 = 1/2, \tau = 0.001, N_B = 0.1, N_{S,1} = 0.001, N_{S,2} = 0.01$. The EA rate region in Ineq. (4) (cyan solid), evaluated on TMSV states, is bounded by the EA outer bound (magenta dashed) in Ineqs. (10); while the coherent-state rate region (black solid) given by Ineq. (8) is bounded by the classical outer bound (black dashed).

We begin with a two-sender case ($s = 2$). As shown in Fig. 4, in all the parameter settings being considered, we can see strict advantages of the EA capacity region (cyan solid) over the classical outer bound (black dashed), which is higher than the coherent-state rate region (black solid). We find that the advantage is larger when the noise N_B is larger, comparing subplots (c) and (d). In particular, this advantage also holds when $N_S \ll N_B \ll 1$, which can happen in the long wavelength infrared domain, as shown in subplot (d).

Comparing with the EA outer bound (magenta dashed), we see that in Fig. 4(a) the TMSV rate region (cyan solid) touches the EA outer bound (magenta dashed) at a corner point when $R_2/C_{\text{coh}}^2 = R_1/C_{\text{coh}}^1$ to the leading order. The gap is of the order of 10^{-5} relatively; therefore, at this point, the TMSV source is in fact optimal for the thermal-loss MAC being considered, for this symmetric case where the parameters $N_{S,k} \ll 1$ are identical among the senders. Note this holds although the transmissivities of the senders η_k are not equal. In other cases, when $N_{S,1} \neq N_{S,2}$, regardless of the values of η_k being equal, a strict gap between the TMSV rate

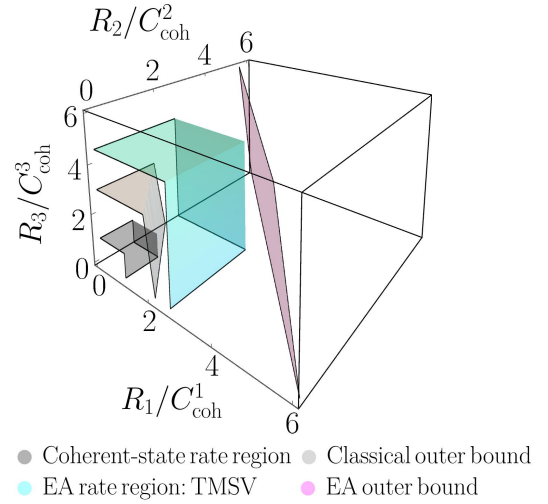


Figure 5. **The asymmetric three-sender EA rate region.** The rates are normalized by the coherent state bound $C_{\text{coh}}^1, C_{\text{coh}}^2$ and C_{coh}^3 defined in Ineq. (8), evaluated in the scenario of microwave domain $N_{S,1} = N_{S,2} = 0.1, N_{S,3} = 0.01, \tau = 0.01, N_B = 20, \eta_1 = \eta_2 = \eta_3 = 1/3$. The EA rate region in Ineq. (4) (cyan), evaluated on TMSV states, is bounded by the EA outer bound (magenta) in Ineqs. (10); while the coherent-state rate region (black) given by Ineq. (8) is bounded by the classical outer bound (light gray).

region and the EA outer bound exists. This does not conclude that the TMSV encoding is inferior, though, as the outer bound is likely to be loose.

Furthermore, we consider a three-sender asymmetric case ($s = 3$), with unequal source brightness $N_{S,1} = N_{S,2} \neq N_{S,3}$. In Fig. 5, a gap emerges between the TMSV rate region (the region below the cyan surface) and the outer bound (the magenta surface), as we expected. An appreciable EA advantage remains as the EA capacity region is several times larger than the coherent state rate region (dark gray surface) and the classical outer bound (light gray surface).

Now we further consider the scaling of the EA advantage observed above. As shown in Fig. 6, the advantage of the EA capacity (magenta) relative to the case without EA also diverges with $\log(N_S)$, when the signal brightness N_S is small and the noise N_B is much larger than the signal brightness N_S . Note that this advantage also holds for the case when $N_S \ll N_B < 1$, as shown in Fig. 6(b). This logarithmic diverging EA advantage in MAC is similar to the single-sender single-receiver case studied in Ref. [28]. Indeed, at the limit $\tau \ll 1, N_S \ll 1$, the relative ratio of the outer bound over the coherent-state rate

$$\frac{C_E(N_{S,k}; \mathcal{L}^{\tau, N_B})}{C_{\text{coh}}^k} \simeq \frac{\log(1/N_{S,k})}{\eta_k(1 + N_B) \log(1 + 1/N_B)}, \quad (12)$$

is also logarithmic in $1/N_{S,k}$ when N_B is small.

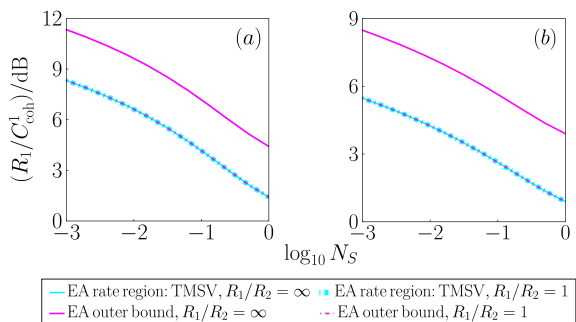


Figure 6. **Rates versus signal brightness.** The dependence on source brightness $N_{S,1} = N_{S,2} = N_S$ of the EA advantage of the EA rate regions for two-sender MAC communication under the scenario of (a) microwave domain $\eta = 1/2, \tau = 0.01, N_B = 20$; (b) long wavelength infrared domain $\eta_1 = \eta_2 = 1/2, \tau = 0.001, N_B = 0.1$. We plot R_1 for sender 1 under conditions $R_1/R_2 = \infty$ (solid) and $R_1/R_2 = 1$ (dot-dashed). For TMSV, the two curves overlap. Note that $R_1/R_2 = 0, \infty$ are equivalent up to a swap due to the symmetry between the two senders; and for given R_1/R_2 , $R_2/C_{\text{coh}}^2 = R_1/C_{\text{coh}}^1$. We also compare the EA rate region of TMSV (cyan) with the EA outer bound (magenta).

C. Protocol designs for the bosonic EA-MAC

In this section, we design a practical protocol to realize EA classical communication over the bosonic thermal-loss MAC. The protocol consists of phase-modulation encoding on the TMSV entanglement source and structured receiver designs.

1. Encoding and receiver designs

Similar to the single-sender single-receiver case, to encode a bit of information $m_k = 0, 1$, the k th sender performs a phase modulation on the signal part of the TMSV pairs via a unitary $\mathcal{E}_{m_k} = e^{im_k \pi \hat{a}_{A_k}^\dagger \hat{a}_{A_k}}$ to produce the quantum system A_k input to the MAC, while the idler part of the TMSV pair A'_k is pre-shared to the receiver side for EA. Here we have considered the binary phase-shift keying: the k th sender sends the bit message $m_k = 0, 1$ by the same probability $p_0 = p_1 = 1/2$. To enable efficient decoding, we consider N_R repetition of such encoding—each message is repeatedly encoded on N_R signal modes of a single sender.

The decoding process takes the output of the MAC \hat{a}_B and the EA idlers $\{\hat{a}_{A'_k}, 1 \leq k \leq s\}$ to decode the information $\{m_k, 1 \leq k \leq s\}$ of all the senders. Below we propose four receiver designs for the decoding. The basic element in the receiver design is the optical parametric amplifier (OPA), which upon input modes \hat{a}_R and \hat{a}_I , produces two modes $\hat{a}'_R = \sqrt{G}\hat{a}_R + \sqrt{G-1}\hat{a}_I^\dagger, \hat{a}'_I = \sqrt{G}\hat{a}_I + \sqrt{G-1}\hat{a}_R^\dagger$, where G is the gain of the OPA. An OPA transforms the phase-sensitive correlation between

the input mode-pair into the photon number difference $\Delta \langle \hat{a}'_I \hat{a}'_I \rangle \propto \sqrt{G(G-1)} 2\text{Re} \langle \hat{a}_I \hat{a}_R \rangle$, which is widely utilized to design receivers in EA applications, such as quantum illumination [51] and the bipartite EA classical communication [28]. Moreover, one can use an OPA as a phase-conjugator to design a phase-conjugate receiver (PCR), as explained in Ref. [28].

To decode all s messages, one can apply two different strategies, either decode them in a serial manner or in parallel. One can also base the receiver design on the direct OPA or on the phase-conjugation mechanism. These choices lead to four receiver designs—serial OPA receiver (OPAR), serial PCR, parallel OPAR and parallel PCR—as we summarize below (see details in Appendix B).

In the serially connected scheme, on the k th round, the signal output $\hat{a}'_{B_{k-1}}$ from the $(k-1)$ th round and the idler \hat{a}_{A_k} are input to an OPA. The idler mode output from the OPA is detected, by direct detection in serial OPAR or an interferometric detection in serial PCR, to decode the message from the k th sender. Meanwhile, the signal mode output from the OPA is further utilized in the next round. Note that after the k th round, the cross correlation between the signal mode with the other idler modes are almost intact; therefore, performing an OPA on the signal and another idler $\hat{a}_{A'_k}$, one can decode the message from the k' th sender. Iterating this procedure on the remaining mode consecutively, one obtains a serial architecture for the receiver, as shown in Fig. 7 (a)(b) for the serial OPAR and serial PCR.

We can also adopt a parallel design for the receivers. As the thermal-loss channel in the MAC adds excess noise into the output, we expect that in the noisy case, splitting the received signal into s copies, each for the decoding of the message of a single sender, will still provide similar signal-to-noise ratios (SNR), when compared to the case without the splitting. In this way, each portion of the received signal can be utilized in parallel, in each individual OPA component in the parallel OPAR or in each phase-conjugation detection in the parallel PCR, to decode each message. As shown in Fig. 7 (c)(d), we can design parallel-OPAR and parallel-PCR schemes.

Finally, we specify the choices of the gain in the OPA. Optimized with respect to the SNR, for OPAR the gains of the s OPAs are to be $G_k = \sqrt{N_{S,k}}/\sqrt{N_B(1+N_B)}$, $1 \leq k \leq s$. For PCR the optimal gain turns out to be at infinity; however, we find that the performance is saturated when $(G_k - 1)N_B \gg N_{S,k}$ for the k th sender, thus we choose a feasible value accordingly.

2. Receiver rate region evaluations

As the encoding and receivers are chosen, now the (soft-decoding) rate region is entirely obtained from the classical formula of conditional mutual information [2] computed over the measurement outcome distribution (see Appendix B). As shown in Fig. 8, we compare the re-

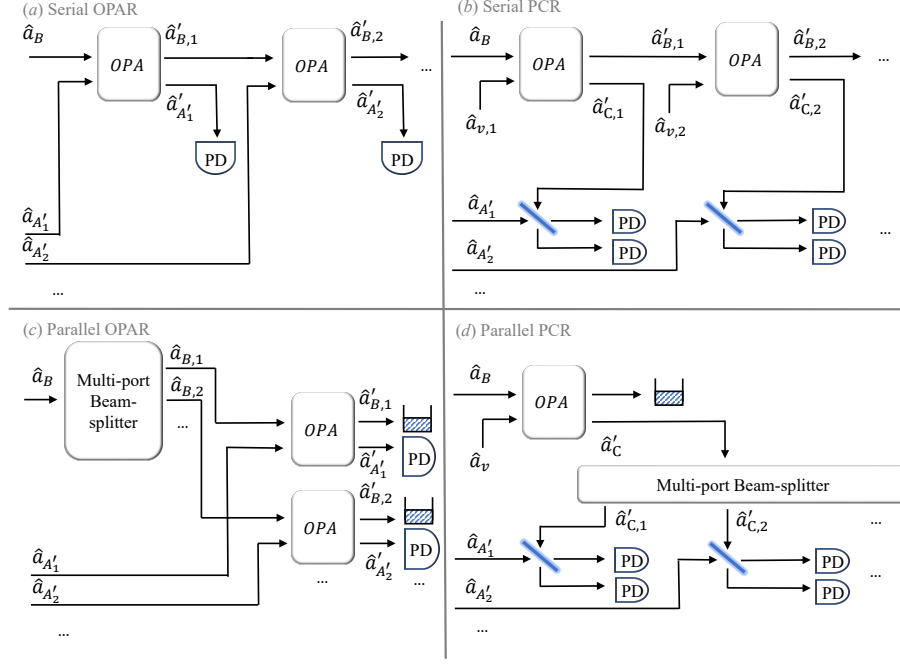


Figure 7. **Schematic of four receiver designs.** (a) serial optical-parametric-amplifier receiver (sOPAR) (b) serial phase-conjugate receiver (sPCR) (c) parallel optical-parametric-amplifier receiver (pOPAR) (d) parallel phase-conjugate receiver (pPCR).

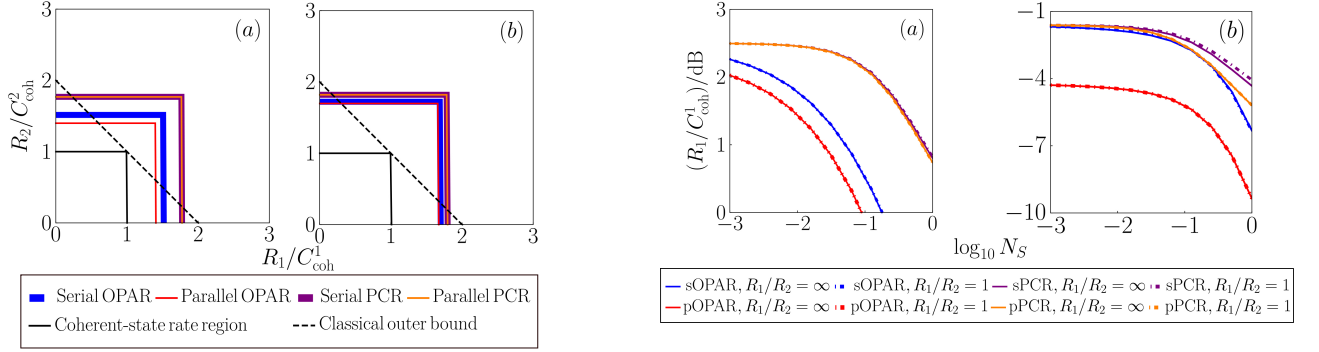


Figure 8. **The two-sender rate region of our four receivers.** The rates are normalized by the coherent state bound $C_{\text{coh}}^1, C_{\text{coh}}^2$ defined in Ineq. (8): (a) microwave domain $N_{S,1} = N_{S,2} = 0.01, \tau = 0.01, N_B = 20, \eta_1 = \eta_2 = 1/2, N_R = 2 \times 10^4$; (b) a noisy channel with $N_{S,1} = N_{S,2} = 10^{-3}, \tau = 10^{-3}, N_B = 10^4, \eta = 1/2, N_R = 10^7$. To distinguish between the overlapping lines, we plot the serial receivers in thicker lines by contrast with the parallel receivers plotted narrowed. The gains of OPAR are given in the main text, and the gains of PCR are $G = 2$ for $N_B = 20$ and $G = 1 + 10^{-3}$ for $N_B = 10^4$. We also compare the receiver rate region with the coherent-state rate (black solid) region and the classical outer bound (black dashed).

ceiver rate regions with the classical coherent-state rate region in Ineq. (8) (black solid) and the classical outer bound in Ineq. (9) jointly and Ineq. (8) (black dashed)

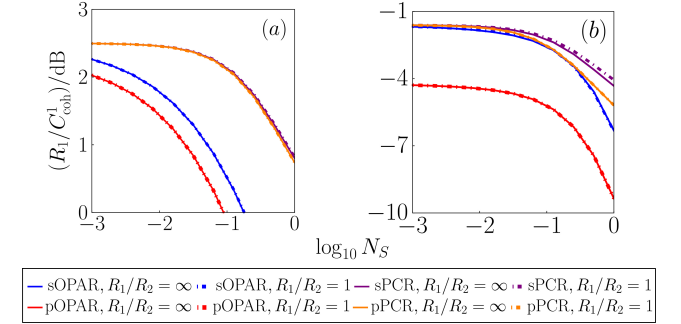


Figure 9. **Receiver rates versus signal brightness.** The dependence on source brightness $N_{S,1} = N_{S,2} = N_S$ of the EA advantage of the four receivers for two-sender MAC communication under the scenario of (a) microwave domain $\eta = 1/2, \tau = 0.01, N_B = 20$; (b) long wavelength infrared domain $\eta_1 = \eta_2 = 1/2, \tau = 0.001, N_B = 0.1$. In the legend s, p refer to ‘serial’ and ‘parallel’ respectively. The number of modes N_R is fixed such that the SNR $N_R \tau N_S / N_B = 0.1$ for sender $i = 1, 2$. We plot R_1 for sender 1 under conditions $R_1/R_2 = \infty$ (solid) and $R_1/R_2 = 1$ (dot-dashed). Note that $R_1/R_2 = 0, \infty$ are equivalent up to a swap due to the symmetry between the two senders; and for given $R_1/R_2, R_2/C_{\text{coh}}^2 = R_1/C_{\text{coh}}^1$.

with J being all senders. We see that the performance of both OPAR and PCR can beat the classical coherent state rate region and the classical outer bound.

In Fig. 8, the performance of the OPAR (blue solid and

red solid) is inferior to the PCR (purple solid and orange solid), a gap between which is significant in Fig. 8(a). This is because the PCR has a better SNR to the next order in N_S compared with OPA, as found in the single-sender case in Ref. [28] and confirmed in Fig. 9 here. As the brightness N_S decreases in Fig. 8(b), the gap between the PCR and OPA almost diminishes. In Fig. 9, we see the rates of OPA (blue and red) are lower than PCR (purple and orange), with a gap expanding as the brightness N_S grows. We also find that the rate advantage of both the OPA and PCR saturates to 3dB as the brightness N_S decreases, consistent with the SNR advantage in quantum illumination [48, 49]. This is because when the noise is large, the information rate is proportional to the SNR. Note that when the channel noise N_B decreases, the theoretical EA advantage evaluated by TMSV remains substantial. However, the practical advantage allowed by our receivers diminishes as N_B falls below 1. For $N_B = 0.1$ (and smaller), there is no advantage for the proposed receivers, as shown in Fig. 9(b). This leaves an open question that a feasible receiver that provides EA advantage in the low-noise scenario is hitherto elusive.

III. DISCUSSION

In this paper, we have solved the capacity region of entanglement-assisted classical communication over a quantum multiple-access channel with an arbitrary number of senders. We also provide explicit encoding and decoding strategies that offer a practical route towards achieving quantum advantages in such network commu-

nication scenarios. Due to teleportation [45] and superdense coding [12], the rate region of EA quantum communication is precisely half of the EA classical communication region; therefore, all of our results can be straightforwardly extended to the case of quantum communication. The explicit protocols can also be used for EA quantum communication via further combining with a teleportation protocol.

Many future directions can be explored. For example, multi-partite entanglement may be considered instead of the product form of Eq. (1) to assist the communication scenario, when the senders can collaborate in the entanglement distribution process. Another open question is whether one can have superadditivity phenomena in our entanglement-assisted capacity region of multiple-access channels.

Before closing, we discuss potential experimental realizations for the proposed EA-MAC communication systems. The basic setup will be similar to that in Ref. [27], with entanglement generated by spontaneous parametric down-conversion in a nonlinear crystal. The receiver can be implemented with another nonlinear crystal to perform phase conjugation or parametric amplification. However, the challenge to demonstrate an entanglement advantage under the multiple-senders scenario is that the pump beams for different entanglement sources need to be frequency and phase locked. Moreover, each stored idler needs to be phase locked to its corresponding signal received from the MAC. Differential-phase encoding can potentially avoid the need for phase locking, which is subject to future studies.

-
- [1] C. Shannon, A mathematical theory of communication bell, Syst. Tech. J. **27**, 379 (1948).
 - [2] T. M. Cover, *Elements of information theory* (John Wiley & Sons, 1999).
 - [3] P. Hausladen, R. Jozsa, B. Schumacher, M. Westmoreland, and W. K. Wootters, Classical information capacity of a quantum channel, Phys. Rev. A **54**, 1869 (1996).
 - [4] B. Schumacher and M. D. Westmoreland, Sending classical information via noisy quantum channels, Phys. Rev. A **56**, 131 (1997).
 - [5] A. S. Holevo, The capacity of the quantum channel with general signal states, IEEE Trans. Inf. Theory **44**, 269 (1998).
 - [6] M. B. Hastings, Superadditivity of communication capacity using entangled inputs, Nat. Phys. **5**, 255 (2009).
 - [7] G. Smith and J. Yard, Quantum communication with zero-capacity channels, Science **321**, 1812 (2008).
 - [8] E. Y. Zhu, Q. Zhuang, and P. W. Shor, Superadditivity of the classical capacity with limited entanglement assistance, Phys. Rev. Lett. **119**, 040503 (2017).
 - [9] E. Y. Zhu, Q. Zhuang, M.-H. Hsieh, and P. W. Shor, Superadditivity in trade-off capacities of quantum channels, IEEE Trans. Inf. Theory (2018).
 - [10] F. Leditzky, D. Leung, and G. Smith, Dephasing channel and superadditivity of coherent information, Phys. Rev. Lett. **121**, 160501 (2018).
 - [11] M. Fanizza, F. Kianvash, and V. Giovannetti, Quantum flags and new bounds on the quantum capacity of the depolarizing channel, Phys. Rev. Lett. **125**, 020503 (2020).
 - [12] C. H. Bennett and S. J. Wiesner, Communication via one-and two-particle operators on einstein-podolsky-rosen states, Phys. Rev. Lett. **69**, 2881 (1992).
 - [13] C. H. Bennett, P. W. Shor, J. A. Smolin, and A. V. Thapliyal, Entanglement-assisted classical capacity of noisy quantum channels, Phys. Rev. Lett. **83**, 3081 (1999).
 - [14] C. H. Bennett, P. W. Shor, J. A. Smolin, and A. V. Thapliyal, Entanglement-assisted capacity of a quantum channel and the reverse shannon theorem, IEEE Trans. Inf. Theory **48**, 2637 (2002).
 - [15] A. S. Holevo, On entanglement-assisted classical capacity, J. Math. Phys. **43**, 4326 (2002).
 - [16] P. W. Shor, The classical capacity achievable by a quantum channel assisted by limited entanglement. Preprint at <https://arxiv.org/abs/quant-ph/0402129> (2004).
 - [17] M.-H. Hsieh, I. Devetak, and A. Winter, Entanglement-assisted capacity of quantum multiple-access channels, IEEE Trans. Inf. Theory **54**, 3078 (2008).
 - [18] Q. Zhuang, E. Y. Zhu, and P. W. Shor, Additive classical

- capacity of quantum channels assisted by noisy entanglement, *Phys. Rev. Lett.* **118**, 200503 (2017).
- [19] M. M. Wilde and M.-H. Hsieh, The quantum dynamic capacity formula of a quantum channel, *Quantum Inf. Process.* **11**, 1431 (2012).
- [20] M. M. Wilde, P. Hayden, and S. Guha, Information trade-offs for optical quantum communication, *Phys. Rev. Lett.* **108**, 140501 (2012).
- [21] Q. Zhuang, Quantum-enabled communication without a phase reference, *Phys. Rev. Lett.* **126**, 060502 (2021).
- [22] S. Lloyd, Capacity of the noisy quantum channel, *Phys. Rev. A* **55**, 1613 (1997).
- [23] P. W. Shor, The quantum channel capacity and coherent information, in *lecture notes, MSRI Workshop on Quantum Computation* (2002).
- [24] I. Devetak, The private classical capacity and quantum capacity of a quantum channel, *IEEE Trans. Inf. Theory* **51**, 44 (2005).
- [25] M. M. Wilde and M.-H. Hsieh, The quantum dynamic capacity formula of a quantum channel, *Quantum Inf. Process.* **11**, 1431 (2012).
- [26] M. M. Wilde, P. Hayden, and S. Guha, Quantum trade-off coding for bosonic communication, *Phys. Rev. A* **86**, 062306 (2012).
- [27] S. Hao, H. Shi, W. Li, Q. Zhuang, and Z. Zhang, Entanglement-assisted communication surpassing the ultimate classical capacity, Preprint at <https://arxiv.org/abs/2101.07482> (2021).
- [28] H. Shi, Z. Zhang, and Q. Zhuang, Practical route to entanglement-assisted communication over noisy bosonic channels, *Phys. Rev. Applied* **13**, 034029 (2020).
- [29] S. Guha, Q. Zhuang, and B. A. Bash, Infinite-fold enhancement in communications capacity using pre-shared entanglement, in *2020 ISIT (IEEE, 2020)* pp. 1835–1839.
- [30] C. N. Gagatsos, M. S. Bullock, and B. A. Bash, Covert capacity of bosonic channels, *IEEE J. Sel. Area Inf. Theory* **1**, 555 (2020).
- [31] R. Laurenza and S. Pirandola, General bounds for sender-receiver capacities in multipoint quantum communications, *Phys. Rev. A* **96**, 032318 (2017).
- [32] J. Nötzel, Entanglement-enabled communication, *IEEE J. Sel. Area Inf. Theory* **1**, 401 (2020).
- [33] F. Leditzky, M. A. Alhejji, J. Levin, and G. Smith, Playing games with multiple access channels, *Nat. Commun.* **11**, 1 (2020).
- [34] J. Yard, P. Hayden, and I. Devetak, Capacity theorems for quantum multiple-access channels: Classical-quantum and quantum-quantum capacity regions, *IEEE Trans. Inf. Theory* **54**, 3091 (2008).
- [35] H. Qi, Q. Wang, and M. M. Wilde, Applications of position-based coding to classical communication over quantum channels, *J. Phys. A: Math. Theor.* **51**, 444002 (2018).
- [36] H. J. Kimble, The quantum internet, *Nature* **453**, 1023 (2008).
- [37] J. Biamonte, M. Faccin, and M. De Domenico, Complex networks from classical to quantum, *Commun. Phys.* **2**, 53 (2019).
- [38] S. Wehner, D. Elkouss, and R. Hanson, Quantum internet: A vision for the road ahead, *Science* **362** (2018).
- [39] W. Kozłowski and S. Wehner, Towards large-scale quantum networks, in *Proceedings of the Sixth Annual ACM International Conference on Nanoscale Computing and Communication* (2019) pp. 1–7.
- [40] B. Zhang and Q. Zhuang, Entanglement formation in continuous-variable random quantum networks, *npj Quantum Inf.* **7**, 33 (2021).
- [41] A. Winter, The capacity of the quantum multiple-access channel, *IEEE Trans. Inf. Theory* **47**, 3059 (2001).
- [42] L. Czekaj and P. Horodecki, Purely quantum superadditivity of classical capacities of quantum multiple access channels, *Phys. Rev. Lett.* **102**, 110505 (2009).
- [43] L. Czekaj, Subadditivity of the minimum output entropy and superactivation of the classical capacity of quantum multiple access channels, *Phys. Rev. A* **83**, 042304 (2011).
- [44] B. J. Yen and J. H. Shapiro, Multiple-access bosonic communications, *Phys. Rev. A* **72**, 062312 (2005).
- [45] C. H. Bennett, G. Brassard, C. Crépeau, R. Jozsa, A. Peres, and W. K. Wootters, Teleporting an unknown quantum state via dual classical and einstein-podolsky-rosen channels, *Phys. Rev. Lett.* **70**, 1895 (1993).
- [46] K. Banaszek, L. Kunz, M. Jarzyna, and M. Jachura, Approaching the ultimate capacity limit in deep-space optical communication, *Proc. SPIE 10910, Free-Space Laser Communications XXXI*, 109100A (2019).
- [47] M. Z. Win and R. A. Scholtz, Ultra-wide bandwidth time-hopping spread-spectrum impulse radio for wireless multiple-access communications, *IEEE Trans. Inf. Theory* **48**, 679 (2000).
- [48] S.-H. Tan, B. I. Erkmen, V. Giovannetti, S. Guha, S. Lloyd, L. Maccone, S. Pirandola, and J. H. Shapiro, Quantum illumination with gaussian states, *Phys. Rev. Lett.* **101**, 253601 (2008).
- [49] Q. Zhuang, Z. Zhang, and J. H. Shapiro, Optimum mixed-state discrimination for noisy entanglement-enhanced sensing, *Phys. Rev. Lett.* **118**, 040801 (2017).
- [50] V. Giovannetti, R. Garcia-Patron, N. J. Cerf, and A. S. Holevo, Ultimate classical communication rates of quantum optical channels, *Nat. Photonics* **8**, 796 (2014).
- [51] S. Guha and B. I. Erkmen, Gaussian-state quantum-illumination receivers for target detection, *Phys. Rev. A* **80**, 052310 (2009).

Appendix A: Details of formalism

1. Formal analysis of the EA MAC

In the MAC communication scenario of Fig. 2, each encoded signal-idler is in a state $\hat{\sigma}_{A_k A'_k}^{m_k} = \mathcal{E}_{m_k} \otimes \mathcal{I} \left(\hat{\phi}_{A_k A'_k} \right)$, where \mathcal{I} is the identity channel modeling the ideal storage of the idler system. Denote the overall encoding operation as $\mathcal{E}_m = \otimes_{k=1}^s \mathcal{E}_{m_k}$, and the probability of sending each message as $p_m = \prod_{k=1}^s p_{m_k}$, the overall encoding can be described by the composite quantum state

$$\hat{\Xi}_{MAA'} = \sum_m p_m |m\rangle\langle m|_M \otimes \hat{\sigma}_{AA'}^m, \quad (\text{A1})$$

where $\hat{\sigma}_{AA'}^m = \otimes_{k=1}^s \hat{\sigma}_{A_k A'_k}^{m_k} \equiv [\mathcal{E}_m \otimes \mathcal{I}] \left(\hat{\phi}_{AA'} \right)$ is the overall encoded state conditioned on message m and $|m\rangle\langle m|_M$ is the classical register for message m .

After the encoding, all of the quantum systems from the s senders A are input to the MAC $\mathcal{N}_{A \rightarrow B}$, which outputs the quantum system B for the receiver to decode

the messages jointly with the EA A' . The overall state after the channel is

$$\hat{\omega}_{MBA'} = \sum_m p_m |m\rangle\langle m|_M \otimes \hat{\beta}_{BA'}^m, \quad (\text{A2})$$

where $\hat{\beta}_{BA'}^m = [\mathcal{N}_{A \rightarrow B} \otimes \mathcal{I}] (\hat{\sigma}_{AA'}^m)$.

The performance metric of a communication scenario over a MAC is described by a vector of rates (R_1, \dots, R_s) , where R_k is the reliable communication rate between the k th sender and the receiver. These rates in general have non-trivial trade-offs with each other. Formally, we define an $(n, R_1, \dots, R_s, \epsilon)$ EA code by: the prior set $\{p_{\mathbf{m}_k^n}\}$, the encoded quantum states $\{\hat{\sigma}_{\mathbf{m}_k^n}\}$, $1 \leq k \leq s$ on \mathbf{A}^n , with each message $\mathbf{m}_k^n \in [2^{nR_k}]$, and the decoding positive operator-valued measure (POVM) $\{\hat{\Lambda}_{m_1 \dots m_s}\}$ on $\mathbf{B}^n \mathbf{A}'^n$ such that

$$\text{Tr} \left\{ \hat{\Lambda}_{m_1 \dots m_s} [\mathcal{N}^{\otimes n} \circ (\otimes_{k=1}^s \mathcal{E}_{m_k}) \otimes \mathcal{I}_{\mathbf{A}'^n}] \hat{\phi}_{\mathbf{A}^n \mathbf{A}'^n} \right\} \geq 1 - \epsilon. \quad (\text{A3})$$

We say that (R_1, \dots, R_s) is an achievable rate vector if for all $\epsilon > 0, \delta > 0$ and sufficiently large n , there exists an $(n, R_1 - \delta, \dots, R_s - \delta, \epsilon)$ EA code. The EA classical capacity region $\mathcal{C}_E(\mathcal{N})$ is defined to be the closure of the set of all achievable rate vectors. The regularized capacity $\mathcal{C}_E(\mathcal{N})$ is the union of all ℓ -letter one-shot capacity regions $\mathcal{C}_E^{(1)}(\mathcal{N}^{\otimes \ell})/\ell$, with integers $\ell \geq 1$. The one-shot capacity region $\mathcal{C}_E^{(1)}(\mathcal{N})$ is the closure of the subset of achievable rate vectors by $(n, R_1 - \delta, \dots, R_s - \delta, \epsilon)$ codes that are generated from separable inputs among the n channel uses. Here ‘‘one-shot’’ is in the sense that the entanglement is constrained in a single channel use. In this regard, the capacity region $\mathcal{C}_E^{(1)}(\mathcal{N}^{\otimes \ell})$ considers $\mathcal{N}^{\otimes \ell}$ as a single channel and allows codes with entanglement between ℓ uses of \mathcal{N} . In the case without EA, the capacity region is well-established by the pioneering work of Winter [41] (see Appendix C).

2. Outer bounds for bosonic thermal-loss MAC

Now we provide the outer bound in Ineqs. (10) for the EA classical capacity region of the bosonic thermal-loss MAC. As we see in Fig. 3, the overall channel can be written as a concatenation of two parts, $\mathcal{N} = \mathcal{L}^{\tau, N_B} \circ \mathcal{E}_{\text{MAC}}$, where \mathcal{E}_{MAC} represents the beamsplitter modeling the signal interference. From the bottleneck inequality, the overall communication rate is upper bounded by

$$\sum_{k=1}^s R_k \leq C_E \left(\sum_{k=1}^s \eta_k N_{S,k}; \mathcal{L}^{\tau, N_B} \right), \quad (\text{A4})$$

the single-sender single-receiver EA classical capacity of the thermal-loss channel \mathcal{L}^{τ, N_B} with brightness

$\sum_{k=1}^s \eta_k N_{S,k}$. This is because for the channel \mathcal{L}^{τ, N_B} , only a single mode signal $\hat{a}_{A_{\text{mix}}}$ in Eq. (5) with brightness $\langle \hat{a}_{A_{\text{mix}}}^\dagger \hat{a}_{A_{\text{mix}}} \rangle = \sum_{k=1}^s \eta_k N_{S,k}$ goes through. Explicitly, the capacity

$$C_E(N_S; \mathcal{L}^{\tau, N_B}) = g(N_S) + g(N'_S) - g(A_+) - g(A_-), \quad (\text{A5})$$

with $A_\pm = (D - 1 \pm (N'_S - N_S))/2$, $N'_S = \tau N_S + N_B$ and $D = \sqrt{(N_S + N'_S + 1)^2 - 4\tau N_S(N_S + 1)}$. This proves Ineq. (10b).

As for the individual upper bounds for the senders in Ineq. (10a), we consider a theoretical super-receiver with access to all of the output ports of the beamsplitter part. The super-receiver performs the reverse of the beamsplitter transform, after which the communication reduces to the single-sender scenario of which the information rate is bounded by each single-sender single-receiver EA classical capacity. Explicitly, we have

$$R_k \leq C_E(N_{S,k}; \mathcal{L}^{\tau, N_B}), \quad 1 \leq k \leq s, \quad (\text{A6})$$

which proves Ineq. (10a).

Appendix B: Analyses of the receiver designs

To begin with, we briefly summarize the receiver problem to be solved in this section. Note that in this section, we will write subscripts inside subscripts as normal texts so that the equations are not too small to be visible. In the phase encoding scheme, each sender applies a phase rotation on the signal mode \hat{a}_{A_k} of its TMSV source, which modulates the signal-idler correlations by $\langle \hat{a}_{A_k} \hat{a}_{A'_k} \rangle = C_{pk} \equiv \sqrt{N_{S,k}(N_{S,k} + 1)} e^{i\theta_k}$. For binary encoding, each θ_k has two possible values $\theta_k^{(0)} = 0, \theta_k^{(1)} = \pi$. The signal modes \hat{a}_{A_k} then goes through the thermal-loss MAC, which produces the received mode mode \hat{a}_B given by Eq. (5) and Eq. (6) of the main paper.

Below we assess the receivers in the two-sender scenario as an example. The s -sender case is solved in the same way. For convenience, let $\eta_1 = \eta, \eta_2 = 1 - \eta$. To ease the reading, we mark the modes after the OPAs with the superscript ‘ \prime ’.

In the BPSK encoding of all senders, denote the phases of the s senders as $\boldsymbol{\theta}^{(m)}$ conditioned on the message m . The phase-modulated photon statistics $P(\mathbf{n}|\boldsymbol{\theta}^{(m)})$ of the measurement is derived in each subsections. It is convenient to define the photon statistics with respect to the message m : $P(\mathbf{n}|m) \equiv P(\mathbf{n}|\boldsymbol{\theta}^{(m)})$. Define the measurement register space of system B as B_R , then the conditional Shannon information $I(M[J]; B_R|M[J^c])$ can be obtained from the measurement statistics $P(\mathbf{n}|m)$

$$I(M[J]; B_R | M[J^c]) = \sum_{m[J^c]} p_{m[J^c]} \left\{ H \left[\left\{ \sum_{m[J]} p_{m[J]} P(\mathbf{n}|m) \right\}_{\mathbf{n}} \right] - \sum_{m[J]} p_{m[J]} H[\{P(\mathbf{n}|m)\}_{\mathbf{n}}] \right\}, \quad (\text{B1})$$

where $H[\{P(\mathbf{n})\}_{\mathbf{n}}] = -\sum_{\mathbf{n}} P(\mathbf{n}) \log P(\mathbf{n})$ is the Shannon entropy of the distribution P . Different from the quantity $I(M[J]; B | M[J^c])$, here Eq. (B1) is the formula of the optimum information rate for a specific measurement strategy given by one of the four receiver designs.

While the performances of OPAR are evaluated exactly, the performances of PCR are evaluated with a Gaussian approximation on the photon statistics, which is precise when the number of repetition modes N_R is large.

1. Serial OPAR (Fig. 7a of the main paper)

For the first OPA with a gain G_1 ,

$$\begin{aligned} \hat{a}'_{B,1} &= \sqrt{G_1} \hat{a}_B + \sqrt{G_1 - 1} \hat{a}'_{A_1}{}^\dagger, \\ \hat{a}'_{A_1} &= \sqrt{G_1} \hat{a}_{A_1} + \sqrt{G_1 - 1} \hat{a}'_B. \end{aligned} \quad (\text{B2})$$

We measure the photon counts of N_R independent and identical (i.i.d.) copies of \hat{a}'_{A_1} .

For the second OPA with a gain G_2 ,

$$\begin{aligned} \hat{a}'_{B,2} &= \sqrt{G_2} \hat{a}'_{B,1} + \sqrt{G_2 - 1} \hat{a}'_{A_2}{}^\dagger \\ \hat{a}'_{A_2} &= \sqrt{G_2} \hat{a}_{A_2} + \sqrt{G_2 - 1} \hat{a}'_{B,1}. \end{aligned} \quad (\text{B3})$$

We measure the photon counts of N_R i.i.d. copies of \hat{a}'_{A_2} .

We make decision on the N_R i.i.d. photon counts of modes $\hat{a}'_{A_1}, \hat{a}'_{A_2}$. Indeed, $\hat{a}'_{A_1}, \hat{a}'_{A_2}$ are in a zero-mean Gaussian state with the covariance matrix

$$V \equiv \left\langle \begin{pmatrix} \hat{a}'_{A_1} \\ \hat{a}'_{A_1}{}^\dagger \\ \hat{a}'_{A_2} \\ \hat{a}'_{A_2}{}^\dagger \end{pmatrix} \begin{pmatrix} \hat{a}'_{A_1}{}^\dagger & \hat{a}'_{A_1} & \hat{a}'_{A_2}{}^\dagger & \hat{a}'_{A_2} \end{pmatrix} \right\rangle = \begin{pmatrix} a+1 & 0 & c & 0 \\ 0 & a & 0 & c^* \\ c^* & 0 & s+1 & 0 \\ 0 & c & 0 & s \end{pmatrix}, \quad (\text{B4})$$

where the constants

$$\begin{aligned} a &= G_1 N_{S,1} + 2\sqrt{(G_1 - 1) G_1 \tau \eta} \operatorname{Re} C_{p1} + (G_1 - 1) [1 + N_B + N_S^*], \\ s &= G_2 N_{S,2} + 2\sqrt{(G_2 - 1) G_2 G_1 \tau (1 - \eta)} \operatorname{Re} C_{p2} \\ &\quad + (G_2 - 1) \left\{ (G_1 - 1) N_{S,1} + G_1 [1 + N_B + N_S^*] + 2 \operatorname{Re} \sqrt{(G_1 - 1) G_1 \tau \eta} C_{p1} \right\}, \\ c &= \sqrt{(G_2 - 1)} \left[\sqrt{(G_1 - 1) G_1} (N_S^* + 1 + N_{S,1}) + (G_1 - 1) \sqrt{\tau \eta} C_{p1}^* + G_1 \sqrt{\tau \eta} C_{p1} \right] + C_{p2}^* \sqrt{\tau \eta G_2 (G_1 - 1)}. \end{aligned} \quad (\text{B5})$$

Here $N_S^* = \tau [N_{S,1} \eta + N_{S,2} (1 - \eta)] + N_B$. The dependence on the phases θ_1, θ_2 lies in the phase-sensitive correlations C_{p1}, C_{p2} .

Given V , we immediately have the covariance matrix of the quadratures $\hat{q}'_{A_k} = \hat{a}'_{A_k} + \hat{a}'_{A_k}{}^\dagger, \hat{p}'_{A_k} = -i(\hat{a}'_{A_k} - \hat{a}'_{A_k}{}^\dagger)$ for the two modes $k = 1, 2$

$$V_{\text{quad}} \equiv \left\langle \begin{pmatrix} \hat{q}_1 \\ \hat{p}_1 \\ \hat{q}_2 \\ \hat{p}_2 \end{pmatrix} \begin{pmatrix} \hat{q}_1 & \hat{p}_1 & \hat{q}_2 & \hat{p}_2 \end{pmatrix} \right\rangle = \begin{pmatrix} E & 0 & C & 0 \\ 0 & E & 0 & C \\ C & 0 & S & 0 \\ 0 & C & 0 & S \end{pmatrix}, \quad (\text{B6})$$

which can be obtained via the relationship $V_{\text{quad}} = UVU^\dagger$ with the transform matrix U

$$U = \begin{pmatrix} 1 & 1 & 0 & 0 \\ -i & i & 0 & 0 \\ 0 & 0 & 1 & 1 \\ 0 & 0 & -i & i \end{pmatrix}. \quad (\text{B7})$$

The probability distribution of the random photon counts of such a two-mode Gaussian state with the

quadrature covariance matrix Eq. (B6) is given by

$$P(n_1, n_2 | \theta_1, \theta_2) = -4F_R(1 + n_1, 1 + n_2, 1, \frac{4C^2}{XY}) \times \frac{(-1 + C^2 + E + S - ES)^{1+n_1+n_2}}{X^{1+n_1}Y^{1+n_2}}, \quad (\text{B8})$$

where F_R is the regularized hypergeometric function and $X = 1 + C^2 + E - (1 + E)S$, $Y = C^2 - (E - 1)(S + 1)$. The information rates are then obtained via Eq. (B1).

2. Serial PCR (Fig. 7b of the main paper)

For the first OPA with a gain G_1 ,

$$\begin{aligned} \hat{a}'_{B,1} &= \sqrt{G_1}\hat{a}_B + \sqrt{G_1 - 1}\hat{a}_{v,1}^\dagger, \\ \hat{a}'_{C,1} &= \sqrt{G_1}\hat{a}_{v,1} + \sqrt{G_1 - 1}\hat{a}'_B, \end{aligned} \quad (\text{B9})$$

$$V \equiv \left\langle \begin{pmatrix} \hat{a}'_{X,1} \\ \hat{a}'_{X,1}^\dagger \\ \hat{a}'_{Y,1} \\ \hat{a}'_{Y,1}^\dagger \\ \hat{a}'_{X,2} \\ \hat{a}'_{X,2}^\dagger \\ \hat{a}'_{Y,2} \\ \hat{a}'_{Y,2}^\dagger \end{pmatrix} \begin{pmatrix} \hat{a}'_{X,1} & \hat{a}'_{X,1} & \hat{a}'_{Y,1} & \hat{a}'_{Y,1} & \hat{a}'_{X,2} & \hat{a}'_{X,2} & \hat{a}'_{Y,2} & \hat{a}'_{Y,2} \end{pmatrix} \right\rangle = \begin{pmatrix} a_1 + 1 & 0 & c_1 & 0 & a_3 & 0 & c_{31} & 0 \\ 0 & a_1 & 0 & c_1^* & 0 & a_3^* & 0 & c_{31}^* \\ c_1^* & 0 & s_1 + 1 & 0 & c_{32} & 0 & s_3 & 0 \\ 0 & c_1 & 0 & s_1 & 0 & c_{32}^* & 0 & s_3^* \\ a_3^* & 0 & c_{32}^* & 0 & a_2 + 1 & 0 & c_2 & 0 \\ 0 & a_3 & 0 & c_{32} & 0 & a_2 & 0 & c_2^* \\ c_{31}^* & 0 & s_3^* & 0 & c_2^* & 0 & s_2 + 1 & 0 \\ 0 & c_{31} & 0 & s_3 & 0 & c_2 & 0 & s_2 \end{pmatrix}, \quad (\text{B11})$$

where the constants

$$\begin{aligned} a_1 &= \frac{1}{2} \left(2 \operatorname{Re}(C_{p1}) \sqrt{\eta(G_1 - 1)\tau} + \eta G_1 \tau N_{S,1} - (\eta - 1)(G_1 - 1)\tau N_{S,2} - \eta \tau N_{S,1} + (G_1 - 1)(N_B + 1) + N_{S,1} \right), \\ s_1 &= \frac{1}{2} \left(-2 \operatorname{Re}(C_{p1}) \sqrt{\eta(G_1 - 1)\tau} + \eta(G_1 - 1)\tau N_{S,1} - (\eta - 1)(G_1 - 1)\tau N_{S,2} + (G_1 - 1)(N_B + 1) + N_{S,1} \right), \\ c_1 &= \frac{1}{2} \left(-2i \operatorname{Im}(C_{p1}) \sqrt{\eta(G_1 - 1)\tau} + \eta(1 - G_1)\tau N_{S,1} + (\eta - 1)(G_1 - 1)\tau N_{S,2} + (1 - G_1)(N_B + 1) + N_{S,1} \right), \\ a_3 &= \frac{1}{2} \left(C_{p2}^* \sqrt{(1 - \eta)(G_1 - 1)\tau} + C_{p1} \sqrt{\eta G_1(G_2 - 1)\tau} + \sqrt{(G_1 - 1)G_1(G_2 - 1)}(N_S^* + 1) \right), \\ s_3 &= \frac{1}{2} \left(-C_{p2}^* \sqrt{(1 - \eta)(G_1 - 1)\tau} + C_{p1} \left(-\sqrt{\eta G_1(G_2 - 1)\tau} \right) + \sqrt{(G_1 - 1)G_1(G_2 - 1)}(N_S^* + 1) \right), \\ c_{31} &= \frac{1}{2} \left(C_{p2}^* \sqrt{(1 - \eta)(G_1 - 1)\tau} + C_{p1} \left(-\sqrt{\eta G_1(G_2 - 1)\tau} \right) - \sqrt{(G_1 - 1)G_1(G_2 - 1)}(N_S^* + 1) \right), \\ c_{32} &= \frac{1}{2} \left(-C_{p2}^* \sqrt{(1 - \eta)(G_1 - 1)\tau} + C_{p1} \sqrt{\eta G_1(G_2 - 1)\tau} - \sqrt{(G_1 - 1)G_1(G_2 - 1)}(N_S^* + 1) \right), \\ a_2 &= \frac{1}{2} \left(2 \operatorname{Re}(C_{p2}) \sqrt{(1 - \eta)G_1(G_2 - 1)\tau} + G_1(G_2 - 1)(N_S^* + 1) + N_{S,2} \right), \\ s_2 &= \frac{1}{2} \left(-2 \operatorname{Re}(C_{p2}) \sqrt{(1 - \eta)G_1(G_2 - 1)\tau} + G_1(G_2 - 1)(N_S^* + 1) + N_{S,2} \right), \\ c_2 &= \frac{1}{2} \left(-2i \operatorname{Im}(C_{p2}) \sqrt{(1 - \eta)G_1(G_2 - 1)\tau} - G_1(G_2 - 1)(N_S^* + 1) + N_{S,2} \right). \end{aligned} \quad (\text{B12})$$

The dependence on phase modulation θ_1, θ_2 lies in the phase-sensitive correlations C_{p1}, C_{p2} .

where the ancilla $\hat{a}_{v,1}$ is in a vacuum mode. The following balanced beamsplitter yields two arms $\hat{a}_{X,1} = (\hat{a}'_{C,1} + \hat{a}_{A_1})/\sqrt{2}$, $\hat{a}_{Y,1} = (\hat{a}'_{C,1} - \hat{a}_{A_1})/\sqrt{2}$. We measure the photon count differences of N_R i.i.d. copies between $\hat{a}_{X,1}$ and $\hat{a}_{Y,1}$.

For the second OPA with a gain G_2 ,

$$\begin{aligned} \hat{a}'_{B,2} &= \sqrt{G_2}\hat{a}'_{B,1} + \sqrt{G_2 - 1}\hat{a}_{v,2}^\dagger, \\ \hat{a}'_{C,2} &= \sqrt{G_2}\hat{a}_{v,2} + \sqrt{G_2 - 1}\hat{a}'_{B,1}. \end{aligned} \quad (\text{B10})$$

Similarly the following balanced beamsplitter yields two arms $\hat{a}_{X,2} = (\hat{a}'_{C,2} + \hat{a}_{A_2})/\sqrt{2}$, $\hat{a}_{Y,2} = (\hat{a}'_{C,2} - \hat{a}_{A_2})/\sqrt{2}$. We measure the photon count differences between $\hat{a}_{X,2}$ and $\hat{a}_{Y,2}$ of N_R i.i.d. copies. The modes $\hat{a}_{X,1}, \hat{a}_{Y,1}, \hat{a}_{X,2}, \hat{a}_{Y,2}$ are in a zero-mean Gaussian state with the covariance matrix

As it is challenging to numerically evaluate the photon count distribution of a four-mode Gaussian state,

we estimate the performance of PCRs by a Gaussian approximation. From the covariance matrix V of $\hat{a}_{X,1}, \hat{a}_{Y,1}, \hat{a}_{X,2}, \hat{a}_{Y,2}$, by Wick's theorem we immediately have the 2×2 covariance matrix V_d of the photon differences $\Delta \hat{N}_i = \hat{N}_{X,i} - \hat{N}_{Y,i} = \langle \hat{a}_{X,i} \hat{a}_{X,i} \rangle - \langle \hat{a}_{Y,i} \hat{a}_{Y,i} \rangle$ for the two slices $i = 1, 2$. Due to the central limit theorem, the mean distribution of N_R i.i.d. copies of random variables $\Delta N_1, \Delta N_2$ converges to the Gaussian distribution when $N_R \rightarrow \infty$

$$P(\mathbf{n}|\theta_1, \theta_2) = \frac{1}{(2\pi)^2 \sqrt{\det V_d^{(N_R)}}} \exp \left\{ -\frac{\mathbf{n}^T V_d^{(N_R)-1} \mathbf{n}}{2} \right\}, \quad (\text{B13})$$

where $V_d^{(N_R)} = V_d/N_R$ is the covariance matrix of the N_R -copy mean distribution, \mathbf{n} is the two-dimensional output averaged over N_R copies of the random photon count differences $\Delta N_1, \Delta N_2$. The information rates are then obtained via Eq. (B1).

$$\begin{aligned} a &= \eta(G_1 - 1)N_B + 2\eta\sqrt{(G_1 - 1)G_1\tau} \operatorname{Re}(C_{p1}) + \eta(G_1 - 1)\tau(\eta N_{S,1} + (1 - \eta)N_{S,2}) + G_1N_{S,1} + G_1 - 1, \\ s &= (G_2 - 1)[(1 - \eta)(N_B + \eta\tau N_{S,1}) + (1 - \eta)^2\tau N_{S,2}] + G_2(N_{S,2} + 1) + 2(\eta - 1)\sqrt{(G_2 - 1)G_2\tau} \operatorname{Re}(C_{p2}) - 1, \\ c &= -\sqrt{(1 - \eta)\eta(G_2 - 1)}\left(\sqrt{G_1 - 1}N_S^* + C_{p1}\sqrt{G_1\tau}\right) + C_{p2}^*\sqrt{-(\eta - 1)\eta(G_1 - 1)G_2\tau}. \end{aligned} \quad (\text{B16})$$

where $N_S^* = \tau[\eta N_{S,1} + (1 - \eta)N_{S,2}] + N_B$. The photon count distribution is given by Eq. (B8) with quadrature covariance matrix evaluated by plugging a, s, c in Eq. (B6). The information rates are then obtained via Eq. (B1).

4. Parallel PCR (Fig. 7d of the main paper)

By contrast with the parallel OPAR, at the receiver side we first apply the phase conjugation by an OPA to obtain

$$\hat{a}'_C = \sqrt{G}\hat{a}_v + \sqrt{G - 1}\hat{a}_{B,i}^\dagger, \quad (\text{B17})$$

where the ancilla \hat{a}_v is in vacuum. Then a beamsplitter slices the mode \hat{a}'_C into two copies $i = 1, 2$,

$$\hat{a}'_{C,i} = \sqrt{\eta_i}\hat{a}'_C + \sqrt{1 - \eta_i}\hat{a}_{v,i}. \quad (\text{B18})$$

For each slice $i = 1, 2$, a balanced beamsplitter yields two arms $\hat{a}_{X,i} = (\hat{a}_{C,i} + \hat{a}_{A'_i})/\sqrt{2}$, $\hat{a}_{Y,i} = (\hat{a}_{C,i} - \hat{a}_{A'_i})/\sqrt{2}$. We measure the photon count differences between $\hat{a}_{X,i}$ and $\hat{a}_{Y,i}$ of N_R i.i.d. copies. Here $\hat{a}_{X,1}, \hat{a}_{Y,1}, \hat{a}_{X,2}, \hat{a}_{Y,2}$ are in a zero-mean Gaussian state with the covariance matrix in the same form of (B11). The evaluation of parameters a_1, s_1, c_1, \dots is straightforward and lengthy, so we omit it here. A Gaussian approximation for the probability distribution of the measurement results follows from Eq. (B13). The information rates are then obtained via Eq. (B1).

3. Parallel OPAR (Fig. 7c of the main paper)

At the receiver side we apply a beamsplitter to slice the received mode \hat{a}_B into two copies $i = 1, 2$

$$\hat{a}_{B,i} = \sqrt{\eta_i}\hat{a}_B + \sqrt{1 - \eta_i}\hat{a}_{v,i}, \quad (\text{B14})$$

where each ancilla $\hat{a}_{v,i}$ is in vacuum. For each OPA $i = 1, 2$

$$\begin{aligned} \hat{a}'_{B,i} &= \sqrt{G_i}\hat{a}_{B,i} + \sqrt{G_i - 1}\hat{a}_{A'_i}^\dagger, \\ \hat{a}'_{A'_i} &= \sqrt{G_i}\hat{a}_{A'_i} + \sqrt{G_i - 1}\hat{a}_{B,i}^\dagger. \end{aligned} \quad (\text{B15})$$

We measure the photon counts of N_R i.i.d. copies of $\hat{a}'_{A'_1}, \hat{a}'_{A'_2}$. These modes are in a Gaussian state with the covariance matrix in the same form of Eq. (B4) valued by

Appendix C: MAC HSW theorem

Consider the s -sender MAC \mathcal{M} . Here we deliberately use a different notation \mathcal{M} instead of \mathcal{N} for reasons that will become apparent later. The scenario of MAC classical communication without EA is similar to the EA case

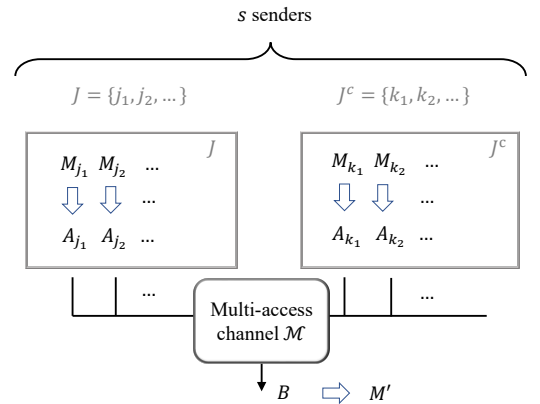


Figure 10. The protocol of general MAC communication. The s senders individually prepare the quantum states in the corresponding quantum system A_i given their messages in each codeword space M_i . The receiver reconstructs a message in codeword space M' decoded from the output in quantum system B .

in Fig. 2 of the main paper, except that the EA systems A' are gone. We also adopt the same notation, as shown in Fig. 10.

The receiver decodes the messages $m = m_1 m_2 \dots m_s$ of all senders, of which the word space is denoted as M' . Accordingly, we can write the message as a bipartition $m = m[J]m[J^c]$. The input encoding of the MAC $\{p_m, \hat{\sigma}_A^m\}$ involves sending each quantum state $\hat{\sigma}_A^m$ through MAC \mathcal{M} by probability p_m . The overall state after the encoding is

$$\hat{\Xi}_{MA} = \sum_m p_m |m\rangle\langle m|_M \otimes \hat{\sigma}_A^m. \quad (\text{C1})$$

Note that due to the independence between the s senders, the overall probability and state of each encoding can be written as the products $p_m = \prod_{i=1}^s p_{m_i}$, $\hat{\sigma}_A^m = \otimes_{i=1}^s \hat{\sigma}_{A_i}^{m_i}$, where A_i denote the quantum system of sender i . Alternatively, for an arbitrary bipartition J, J^c , we have $p_m = p_{m[J]}p_{m[J^c]}$, $\hat{\sigma}_A^m = \hat{\sigma}_{A[J]} \otimes \hat{\sigma}_{A[J^c]}$. The MAC maps the composite input A to a single output quantum system B , leading to the output

$$\hat{\omega}_{MB} = \sum_m p_m |m\rangle\langle m|_M \otimes \mathcal{M}_{A \rightarrow B}(\hat{\sigma}_A^m). \quad (\text{C2})$$

With the above notations prepared, we can introduce the information theoretical quantities. To begin with, we introduce the conditional entropy

$$S(B|M[J^c])_{\hat{\omega}} = \sum_{m[J^c]} p_{m[J^c]} S \left[\mathcal{M}_{A \rightarrow B} \left(\sum_{m[J]} p_{m[J]} \hat{\sigma}_A^m \right) \right], \quad (\text{C3})$$

similarly, noting that $M = M[J]M[J^c]$ and $p_m = p_{m[J]}p_{m[J^c]}$ we can have the notation

$$S(B|M)_{\hat{\omega}} = \sum_m p_m S[\mathcal{M}_{A \rightarrow B}(\hat{\sigma}_A^m)]. \quad (\text{C4})$$

We introduce the conditional quantum mutual information

$$I(M[J]; B|M[J^c])_{\hat{\omega}} = S(B|M[J^c])_{\hat{\omega}} - S(B|M)_{\hat{\omega}} \quad (\text{C5})$$

The one-shot capacity region of the quantum MAC \mathcal{M} can be directly obtained from the classical-quantum channel formalism in Ref. [41]. In this case, we can reduce the $(n, R_1, \dots, R_s, \epsilon)$ code defined in Appendix A to the n -block code proposed in Ref. [41], as we detail below. In the n quantum channel uses, sender k encodes the n -partite codeword \mathbf{w}_k^n from the code space \mathbf{W}_k^n of size 2^{nR_k} . Without loss of generality, we consider each codeword to be chosen with equal probability $p_{\mathbf{w}_k^n} = 1/2^{nR_k}$. A classical n -block coding maps the codewords from \mathbf{W}_k^n to \mathbf{M}_k^n as

$$F : \mathbf{w}_k^n \rightarrow \mathbf{m}_k^n \equiv m_k^{(1)} \dots m_k^{(n)}, 1 \leq k \leq s, \quad (\text{C6})$$

where each block $m_k^{(u)}$ is in the message space $M_k^{(u)}$, the n blocks together form message \mathbf{m}_k^n in \mathbf{M}_k^n . Alternatively, F can be implemented by sending each message \mathbf{m}_k^n subject to probability distribution

$$p_{\mathbf{m}_k^n} = \sum_{\mathbf{w}_k^n \in \mathcal{S}(\mathbf{m}_k^n)} p_{\mathbf{w}_k^n}, \quad (\text{C7})$$

where $\mathcal{S}(\mathbf{m}_k^n)$ is the set spanned by \mathbf{w}_k^n 's satisfying $F(\mathbf{w}_k^n) = \mathbf{m}_k^n$. We define the marginal distribution for each block $p_{m_k^{(u)}}$ for $1 \leq u \leq n$. For the one-shot capacity region, entanglement is forbidden among the n blocks and we consider product states as the encoding

$$\hat{\sigma}^{\mathbf{m}_k^n} = \otimes_{u=1}^n \hat{\sigma}_u^{m_k^{(u)}}, 1 \leq k \leq s, \quad (\text{C8})$$

where $\hat{\sigma}_u^{m_k^{(u)}}$ is the state of the quantum system at the u th block for sender k . Without loss of generality, we can always fix the classical-quantum encoding mapping

$$\mathcal{F}_k : m_k^{(u)} \rightarrow \hat{\sigma}^{m_k^{(u)}}, 1 \leq k \leq s, \quad (\text{C9})$$

for all channel uses $1 \leq u \leq n$. This is because time sharing of different $\{\hat{\sigma}_u^{m_k^{(u)}}\}$'s over $u \in [1, n]$ is available by expanding the domain of $\{m_k^{(u)}\}$ and varying the support of $\{p_{m_k^{(u)}}\}$ per block. As a result, we can always combine the encoding $\{p_{\mathbf{m}_k^n}, \hat{\sigma}^{\mathbf{m}_k^n}\}$ ($1 \leq k \leq s$) with the quantum channel $\mathcal{N}^{\otimes n}$ into an n -block classical-quantum channel $\mathcal{W}^{\otimes n}$, with each classical-quantum channel defined by

$$\mathcal{W} \equiv \mathcal{M} \circ (\otimes_{k=1}^s \mathcal{F}_k) : m_1 m_2 \dots m_s \rightarrow \mathcal{M}(\otimes_{k=1}^s \hat{\sigma}^{m_k}). \quad (\text{C10})$$

To summarize, when considering the one-shot capacity region, a quantum MAC \mathcal{M} with any encoding $\{p_{\mathbf{m}_k^n}, \hat{\sigma}^{\mathbf{m}_k^n}\}$, $1 \leq k \leq s$, can be reduced to a classical-quantum channel \mathcal{W} with certain classical coding F .

With the notations introduced, we restate Theorem 9 and Theorem 10 of Ref. [41] in a version adapted to the communication over a quantum MAC without EA, in preparation for the proof of Theorem 1 of the main paper.

Lemma 2 *Let (R_1, \dots, R_s) be any non-negative-valued vector, satisfying the constraints*

$$\sum_{i \in J} R_i \leq I(M[J]; B|M[J^c])_{\hat{\omega}}, \quad (\text{C11})$$

for some encoding $\{p_{\mathbf{m}_k^n}, \hat{\sigma}^{\mathbf{m}_k^n}\}$, $1 \leq k \leq s$, where $\hat{\omega}$ is defined in Eq. (C2) relying on the encoding. Then, for every $\epsilon, \delta > 0$ and all sufficiently large n , there exists a $(n, R_1 - \delta, \dots, R_s - \delta, \epsilon)$ -code, i.e. (R_1, \dots, R_s) is achievable.

Proof. With the reduction to classical-quantum channel defined by Eq. (C10) and Eq. (C9), this lemma immediately follows from Theorem 9 in Ref. [41]. We note

that the capacity achieving encoding is subject to a product prior distribution $p_{m_k^n} = \prod_{u=1}^n p_{m_k^{(u)}}$, and a product-state encoding $\hat{\sigma}^{m_k^n} = \otimes_{u=1}^n \hat{\sigma}^{m_k^{(u)}}$. ■

Theorem 3 For any s -sender quantum MAC \mathcal{M} , given a constrained set of classical-quantum encoding mappings $\mathcal{F}_k : m_k \rightarrow \hat{\sigma}^{m_k}$, $1 \leq k \leq s$, the one-shot constrained capacity region of reliable classical communication over \mathcal{M} is the convex hull over all rates (R_1, R_2, \dots, R_s) satisfying the 2^s inequalities

$$\sum_{i \in J} R_i \leq I(M[J]; B|M[J^c])_{\hat{\omega}}, \quad (\text{C12})$$

for some encoding $\{p_{m_k}, \hat{\sigma}^{m_k}\}$, $1 \leq k \leq s$. Here $\hat{\omega}$ is defined in Eq. (C2) relying on the encoding.

Proof. The achievability results from Lemma 2, which states that for every $\epsilon, \delta > 0$ and all sufficiently large n , there exists a $(n, R_1 - \delta, \dots, R_s - \delta, \epsilon)$ code (see Appendix A) achieving $I(M[J]; B|M[J^c])_{\hat{\omega}}$. Thus, by time-sharing, Eq. (C12) can always be achieved. Now we address the proof of weak converse here. Considering the classical coding F in, let $\{\{\hat{\sigma}^{w_k^n} \mid 1 \leq k \leq s\}, \{\hat{\Lambda}_{w_1^n \dots w_s^n}\}$ be any $(n, R_1, \dots, R_s, \epsilon)$ code. The channel output is in a separable state

$$\hat{\omega} = \otimes_{k=1}^s \frac{1}{2^{nR_k}} \sum_{w_k^n} (\mathcal{W}^{\otimes n} \circ F)[w_k^n] \otimes |w_k^n\rangle\langle w_k^n|. \quad (\text{C13})$$

Its reduced state in the u th channel use is denoted as $\hat{\omega}^{(u)}$. Denote the error rate of the POVM output $w_k'^n$ as $\epsilon = P(w_k^n \neq w_k'^n)$. By Fano's inequality we have

$$S(\mathbf{W}[J^n | \mathbf{W}'^n])_{\hat{\omega}} \leq 1 + \epsilon n \sum_{i \in J} R_i. \quad (\text{C14})$$

Note that $|w_k^n| = 2^{nR_k}$, $1 \leq k \leq s$. We have

$$\begin{aligned} n \sum_{i \in J} R_i &= S(\mathbf{W}[J^n])_{\hat{\omega}} \\ &= I(\mathbf{W}[J^n]; \mathbf{W}'^n)_{\hat{\omega}} + S(\mathbf{W}[J^n | \mathbf{W}'^n])_{\hat{\omega}} \quad (\text{C15}) \\ &\leq I(\mathbf{W}[J^n]; \mathbf{W}'^n)_{\hat{\omega}} + 1 + \epsilon n \sum_{i \in J} R_i. \end{aligned}$$

For reliable communication we require $\epsilon \rightarrow 0$, thus

$$\begin{aligned} \sum_{i \in J} R_i &\leq \frac{I(\mathbf{W}[J^n]; \mathbf{W}'^n)_{\hat{\omega}}}{n} + \frac{1}{n} \\ &\leq \frac{I(\mathbf{M}[J^n]; \mathbf{B}^n | \mathbf{M}[J^c]^n)_{\hat{\omega}}}{n} + \frac{1}{n} \\ &\leq \frac{\sum_{u=1}^n I(M[J]^{(u)}; B^{(u)} | M[J^c]^{(u)})_{\hat{\omega}^{(u)}}}{n} + \frac{1}{n}, \quad (\text{C16}) \end{aligned}$$

which is outer bounded by the convex hull of rates defined by Eq. (C12). The second inequality is due to the data processing inequality since we have the completely

positive trace-preserving mapping $\mathbf{W}^n \rightarrow \mathbf{M}^n \rightarrow \mathbf{B}^n \rightarrow \mathbf{W}^n$, and that discarding system never increases quantum mutual information (which follows from strong subadditivity of von Neumann entropy); the third inequality results from the chain rule and the fact that $\hat{\omega}$ conditioned on \mathbf{M}^n is a product state over n channel uses. Specifically, choosing the encoding over n blocks to be identical, we have the outer bound of one-encoding rate region defined by

$$\sum_{i \in J} R_i \leq I(M[J]; B|M[J^c])_{\hat{\omega}} + \frac{1}{n}, \quad (\text{C17})$$

■ **Remark.** For an ℓ -letter communication scenario (encoding with inputs entangled between ℓ channel uses), the systems \mathbf{A}^ℓ and \mathbf{B}^ℓ can be entangled over the ℓ letters within a block. In this case, the mutual information is not necessarily subadditive, Eq. (C12) needs to be evaluated over ℓ channel uses as a whole

$$\sum_{i \in J} R_i \leq I(\mathbf{M}[J]^\ell; \mathbf{B}^\ell | \mathbf{M}[J^c]^\ell)_{\hat{\omega}}. \quad (\text{C18})$$

This has already been pointed out in Sec. VII of Ref. [41].

In the EA protocol, the quantum system comes with a reference system A' which is pre-shared to the receiver side intact, while the quantum system goes through the MAC \mathcal{N} . However, we can view the overall channel $\mathcal{M} = \mathcal{N} \otimes \mathcal{I}$ as a single MAC. Note that the encoding is, however, restricted as the \mathcal{I} part corresponds to references. Namely, the encoding mappings are defined by

$$\mathcal{F}_k : m_k \rightarrow \mathcal{E}_{m_k}(\hat{\sigma}^0), \quad 1 \leq k \leq s, \quad (\text{C19})$$

where the generator state $\hat{\sigma}^0$ is an arbitrary state of $A_k A'_k$, while the encoding operations $\{\mathcal{E}_{m_k}\}$ is constrained to act only on the signal system A_k .

Appendix D: Proof of Theorem 1 of the main paper

We derive the EA-MAC classical capacity in analogy to the single-sender single-receiver EA classical capacity [14] and the two-sender EA-MAC classical capacity [17].

Theorem 1 in the maintext includes two parts: the regularization Eq. (2), and the convex hull Eq. (3).

To begin with, we provide an explanation for the regularization. For channel \mathcal{N} , denote $\mathcal{X}(\ell)$ as the set of all codebooks with at most ℓ entangled letters. The ℓ -letter one-shot capacity region $\mathcal{C}_E^{(1)}(\mathcal{N}^{\otimes \ell})$ spans the rate subset achieved by the codebook set $\mathcal{X}(\ell)$. Thus the union of block codes $\bigcup_{\ell=1}^{\infty} \mathcal{X}(\ell)$ includes any possible codebook. Hence the ultimate capacity region $\mathcal{C}_E(\mathcal{N})$ is given by the regularized rate region achieved by the universal codebook set $\bigcup_{\ell=1}^{\infty} \mathcal{X}(\ell)$. This block-code reduction yields Eq. (2) from Eq. (3) in the main text.

Below we provide both the inner and outer bounds of single-letter one-shot region $\mathcal{C}_E^{(1)}(\mathcal{N})$, which coincides and thus gives the formula Eq.(3) in the main text. The proof does not specify the mode number per user since the entanglement assistance is unlimited, thus the formula of ℓ -letter one-shot region $\mathcal{C}_E^{(1)}(\mathcal{N}^{\otimes \ell})$ follows by inserting $\mathcal{N} \rightarrow \mathcal{N}^{\otimes \ell}$, $A \rightarrow \mathbf{A}^\ell$, $B \rightarrow \mathbf{B}^\ell$, A'_k purifying \mathbf{A}_k^ℓ , $1 \leq k \leq s$. The ℓ -letter one-shot, one-state region $\tilde{\mathcal{C}}_E(\mathcal{N}^{\otimes \ell}, \hat{\phi})$ is defined by

$$\sum_{k \in J} R_k \leq I(A'[J]; \mathbf{B}^\ell | A'[J^c])_{\hat{\rho}}, \forall J, \quad (\text{D1})$$

with $\hat{\rho} = \mathcal{N}^{\otimes \ell} \otimes \mathcal{I}(\hat{\phi})$, where $\hat{\phi}$ is a pure state defined on $\mathbf{A}^\ell A'$.

In the proof below, we omit ‘ \wedge ’ in the notation of operators for simplicity, since the meaning of each notation is clear in the context. Our proof combines the techniques in Ref. [41] (Lemma 2 and Theorem 3), Ref. [14], and Ref. [17].

1. Inner bound

We prove the inner bound by showing the boundaries achievable for any pure state ϕ . We show that the 2^s conditional quantum mutual information quantities in Eq. (C12) reach all the boundaries of $\tilde{\mathcal{C}}_E$ region defined by Eq. (4) of the main paper, i.e. the rate region defined by Eq. (C12) is inner bounded by $\tilde{\mathcal{C}}_E$ regions. Lemma 2 guarantees that for any $\epsilon, \delta > 0$ there is some $(n, R_1 - \delta, \dots, R_s - \delta, \epsilon)$ code achieving the region defined by Eq. (C12) with some encoding $\{p_{m_k}, \sigma^{m_k}\}, 1 \leq k \leq s$, thus the convex hull over all possible encodings provides

$$\begin{aligned} \sum_{i \in J} R_i &= I(M[J]; B|M[J^c])_\omega \\ &= \mathbb{E}_{m[J^c]} \left\{ S \left[\mathcal{N} \otimes \mathcal{I} \left(\sum_{m[J]} p_{m[J]} (U_{m[J]} \otimes U_{m[J^c]}) \phi \left(U_{m[J^c]}^\dagger \otimes U_{m[J]}^\dagger \right) \right) \right] - \mathbb{E}_{m[J]} \left\{ S \left[\mathcal{N} \otimes \mathcal{I} (U_m \phi U_m^\dagger) \right] \right\} \right\}, \\ &= \mathbb{E}_{m[J^c]} \left\{ S \left[\mathcal{N} \otimes \mathcal{I} (U_{m[J^c]} \phi_{A'[J^c]A} U_{m[J^c]}^\dagger) \right] + S(\phi_{A'[J]}) - \mathbb{E}_{m[J]} \left\{ S \left[\mathcal{N} \otimes \mathcal{I} (U_m \phi U_m^\dagger) \right] \right\} \right\}, \end{aligned} \quad (\text{D4})$$

where $\mathbb{E}_x[f(x)] \equiv \int dx p(x) f(x)$ refers to the expectation value of function f averaged on probability distribution p . The second equality is because $\{U_{m[J]}\}$ is correlation-removing within system $A[J]$,

$$\mathcal{N} \otimes \mathcal{I} \left(\sum_{m[J]} p_{m[J]} (U_{m[J]} \otimes U_{m[J^c]}) \phi \left(U_{m[J^c]}^\dagger \otimes U_{m[J]}^\dagger \right) \right) = \mathcal{N} \otimes \mathcal{I} (U_{m[J^c]} \phi_{A'[J^c]A} U_{m[J^c]}^\dagger) \otimes \phi_{A'[J]}. \quad (\text{D5})$$

In contrast to the single-user case, here we see that the encoding restricted on $A[J]$ fails to remove the correlation

the inner bound of $\mathcal{C}_E^{(1)}(\mathcal{N})$. Then the achievability of $\text{Conv} \left[\bigcup_{\phi} \tilde{\mathcal{C}}_E(\mathcal{N}, \phi) \right]$ is proven. During the evaluation of entropies within this section, AA' or BA' is the relevant Hilbert space and we omit the subscripts for states living in AA' or BA' .

We begin with the special case of each pair $\{(A_i, A'_i), 1 \leq i \leq s\}$ being in a maximally entangled state, such that the reduced state $\phi_{A_i} = \text{Tr}_{A' A_j \neq i}(\phi) = (I/d_i)_{A_i}$ is fully mixed, here the dimension $d_i = \dim A_i$. The capacity achieving protocol is implemented by a generator state being ϕ and a correlation-removing unitary encoding $\{U_m\}$. In terms of the ensemble $\sum_m p_m U_m \phi U_m^\dagger$, a correlation-removing encoding $\{U_m\}$ wipes out the correlation between each system A_i with its reference system. Concretely, this can be implemented by the generalized Pauli operators

$$\begin{aligned} U_{m_i} &= T_{A_i}^{m_i, T} R_{A_i}^{m_i, R}, \text{ where} \\ m_i &= m_{i, T} m_{i, R}, 1 \leq m_{i, T} \leq d_i, 1 \leq m_{i, R} \leq d_i, \end{aligned} \quad (\text{D2})$$

with the Pauli matrices $T_{jk} = \delta_{j, k-1 \bmod d_i}$, $R_{jk} = e^{i2\pi k/d_i} \delta_{jk}$ acting on each subspace A_i . Governed by the independence constraint of MAC, $\phi = \otimes_{i=1}^s \phi_{A_i A'_i}$. The encoding $U_m = \otimes_{i=1}^s U_{m_i}$ acting on $\otimes_{i=1}^s A_i$ by probability $p_m = \prod_{i=1}^s p_{m_i}$ is also separable, where m_i is subject to the uniform distribution $p_{m_i} = 1/|M_i|$.

Now the overall quantum state after the channel is

$$\omega_{MBA'} = \sum_m p_m |m\rangle\langle m|_M \otimes [\mathcal{N}_{A \rightarrow B} \otimes \mathcal{I}] (U_m \phi U_m^\dagger). \quad (\text{D3})$$

Applying Lemma 2 to Eq. (D3), for any $\epsilon, \delta > 0$ there exists a $(n, R_1 - \delta, \dots, R_s - \delta, \epsilon)$ code achieving the vector of data transmission rate of this protocol

between A and $A'[J^c]$, so $A'[J^c]$ is left with A in the entropy quantities.

Next, we note that for the maximally entangled state ϕ , we have $U \otimes I |\phi\rangle = I \otimes U^* |\phi\rangle$ for any unitary U . This equivalence ensures that the encoding preserves the entropy of the output state

$$\begin{aligned} S \left[\mathcal{N} \otimes \mathcal{I} \left(U_{m[J^c]} \phi_{A'[J^c]A} U_{m[J^c]}^\dagger \right) \right] \\ = S \left[\mathcal{N} \otimes \mathcal{I} \left(\phi_{A'[J^c]A} \right) \right], \end{aligned} \quad (\text{D6})$$

similarly

$$S \left[\mathcal{N} \otimes \mathcal{I} \left(U_m \phi U_m^\dagger \right) \right] = S \left[\mathcal{N} \otimes \mathcal{I} \left(\phi \right) \right]. \quad (\text{D7})$$

Therefore, the averaging in $\mathbb{E}_{m[J]}, \mathbb{E}_{m[J^c]}$ disappears in Eq. (D4). Therefore, Eq. (D4) reduces to

$$\begin{aligned} \sum_{i \in J} R_i = S \left(\mathcal{N} \otimes \mathcal{I} \left(\phi_{A'[J^c]A} \right) \right) + S \left(\phi_{A'[J]} \right) \\ - S \left(\mathcal{N} \otimes \mathcal{I} \left(\phi \right) \right). \end{aligned} \quad (\text{D8})$$

Simplifying the right-hand-side above, we obtain

$$\begin{aligned} \sum_{i \in J} R_i = S \left(B A'[J^c] \right)_\rho + S \left(A'[J] \right)_\rho - S \left(A'[J] B A'[J^c] \right)_\rho \\ = I \left(A'[J]; B A'[J^c] \right)_\rho = I \left(A'[J]; B | A'[J^c] \right)_\rho. \end{aligned} \quad (\text{D9})$$

Here we utilized the channel mapping $\rho = \rho_{B A'} = \mathcal{N}_{A \rightarrow B} \otimes \mathcal{I}(\phi_{A A'})$. The last step is due to independence between the signals. Note that Eq. (D9) holds for any J . Hence Eq. (D4) achieves $\tilde{\mathcal{C}}_E(\mathcal{N}, \phi)$ in Eq. (4) of the main paper for the maximally entangled state.

Indeed, the achievability also holds for any *projection-like* ϕ_A , which is proportional to a projection operator to some subspace \mathcal{S} of the input Hilbert space \mathcal{H}_{in} , along with the encoding $\{U_{m[J]}\}$ restricted on \mathcal{S} . For now, we have achieved the rate region specified by Eq. (4) of the main paper for all projection-like inputs.

Having proven the result for the special case of inputs with a projection-like reduced density matrix, now we extend the proof to general pure product states ϕ . For simplicity here we denote the reduced density matrix as $\xi \equiv \phi_A$. First we introduce the n -block ϵ -typical space $T_n(\xi)$ of an arbitrary single-block state $\xi = \sum_x p(x) |x\rangle\langle x|$, where $\{|x_i\rangle\}$ is an orthogonal set. $T_n(\xi)$ comprises every typical states $|x_1 x_2 \dots x_n\rangle$ associated with typical sequences $x_1 x_2 \dots x_n$ satisfying

$$\left| -\log \left(\prod_{i=1}^n p(x_i) \right) / n - S(\xi) \right| \leq \epsilon. \quad (\text{D10})$$

Denote by P_{T_n} the projection operator onto subspace $T_n(\xi)$. The typicality follows from the law of large number, explicitly, for any $\epsilon > 0$ there exists n sufficiently large such that the typical subspace almost includes the n -block random encoding $\xi^{\otimes n}$

$$\text{Tr} \left[\xi^{\otimes n} (I - P_{T_n}) \right] \leq \delta. \quad (\text{D11})$$

Now let π_{T_n} be the normalized projection operator $P_{T_n} / \dim T_n$. By the definition of ϵ -typicality Eq. (D10),

the entropy of the uniform distribution π_{T_n} is almost $nS(\xi)$ up to a prefactor $\sim 1 - \delta$, explicitly

$$(1 - \delta) 2^{n(S(\xi) - \epsilon)} \leq \dim T_n(\xi) \leq 2^{n(S(\xi) + \epsilon)}. \quad (\text{D12})$$

By a similar correlation-removing encoding on $\Phi_{\pi_{T_n}}$, below we show that the n -block $I(A'[J]^n; B^n | A'[J^c]^n)_{(\mathcal{N} \otimes \mathcal{I})^{\otimes n}(\pi_{T_n})}$ quantity achieves $nI(A'[J]; B | A'[J^c])_{\mathcal{N} \otimes \mathcal{I}(\xi)}$.

Following a similar procedure to the proof for maximally entangled state, Eq. (D8) holds for the n -block state. The typicality Eq. (D12) gives the first term in Eq. (D8). Meanwhile, for the last two terms in Eq. (D8), we construct a unitary including the environment mode to simulate channel \mathcal{N} . Denote the complementary channel as \mathcal{K} , which maps the input state to the environment mode. Define $\Phi_{\pi_{T_n}}$ as a purification of π_{T_n} fulfilled per system pair $A_i A'_i$, $1 \leq i \leq s$. Then the last term $S[(\mathcal{N} \otimes \mathcal{I})^{\otimes n}(\Phi_{\pi_{T_n}})] = S[\mathcal{K}(\pi_{T_n})]$, thereby the latter two terms converges to the desired quantity when $\epsilon \rightarrow 0$

$$\begin{aligned} S \left[\mathcal{N}^{\otimes n} (\pi_{T_n}) \right] - S \left[\mathcal{K} (\pi_{T_n}) \right] \\ \rightarrow n \left[S(\mathcal{N}(\xi)) - S(\mathcal{N} \otimes \mathcal{I}(\Phi_\xi)) \right], \end{aligned} \quad (\text{D13})$$

which follows from Lemma 1 in [14]. Both sides of the equation above can be reduced to a conditional quantum information quantity: $I(A'[J]^n; B^n | A'[J^c]^n)_\rho$ with $\rho = (\mathcal{N} \otimes \mathcal{I})^{\otimes n}(\Phi_{\pi_{T_n}})$ for LHS, and $nI(A'[J]; B | A'[J^c])_\rho$ with $\rho = \mathcal{N} \otimes \mathcal{I}(\phi)$ for RHS. Combining the above together, we have the information rate per letter

$$\begin{aligned} I(A'[J]^n; B^n | A'[J^c]^n)_{(\mathcal{N} \otimes \mathcal{I})^{\otimes n}(\Phi_{\pi_{T_n}})} / n \\ \rightarrow I(A'[J]; B | A'[J^c])_{\mathcal{N} \otimes \mathcal{I}(\phi)} \end{aligned} \quad (\text{D14})$$

given $\epsilon \rightarrow 0$. Note that π_{T_n} is projection-like thus $I(A'[J]^n; B^n | A'[J^c]^n)_{(\mathcal{N} \otimes \mathcal{I})^{\otimes n}(\Phi_{\pi_{T_n}})}$ is achieved by the correlation-removing encoding. Hence, $I(A'[J]; B | A'[J^c])_{\mathcal{N} \otimes \mathcal{I}(\phi)}$ is achievable for any pure product state ϕ .

Now we have proven $\tilde{\mathcal{C}}_E$ specified by Eq. (4) of the main paper is achievable for any input ϕ . Then the convex hull of $\tilde{\mathcal{C}}_E$ is achievable due to time sharing. Thus the one-shot capacity region is inner bounded by the convex hull of $\tilde{\mathcal{C}}_E(\mathcal{N}, \phi)$ regions over all possible ϕ

$$\mathcal{C}_E^{(1)}(\mathcal{N}) \supseteq \text{Conv} \left[\bigcup_{\phi} \tilde{\mathcal{C}}_E(\mathcal{N}, \phi) \right]. \quad (\text{D15})$$

2. Outer bound

Theorem 3 gives an outer bound with a convex hull over the region defined by $I(M[J]; B A' | M[J^c])_\omega$ quantities in Eq. (C12). We prove that $\tilde{\mathcal{C}}_E(\mathcal{N}, \phi)$ is an outer bound of each region defined by Eq. (C12) with repetitive uses of one encoding $\{p_m\}$, which is the outer bound

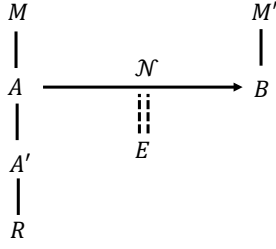


Figure 11. For the proof of the outer bound, A, B are the input and output systems of our MAC \mathcal{N} . M, M' are the input and output code spaces. A' is the entanglement assistance system. System R purifies system A per subsystem A_i , $1 \leq i \leq s$.

of one-shot, one-encoding rates. Then we take the convex hull over $\tilde{\mathcal{C}}_E(\mathcal{N}, \phi)$ and prove it as an outer bound of $\mathcal{C}_E^{(1)}(\mathcal{N})$.

To ease the proof, we introduce reference systems R, E , as shown in Fig. 11. $R = \otimes_{i=1}^s R_i$ individually purifies per sender i the subsystem $\Xi_{M_i A_i A'_i}$ of the overall state $\Xi = \Xi_{MAA'}$ just after encoding, defined by Eq. (A1) of the main paper. The environment system E purifies the overall state, including the system R , just after the channel. The channel is extended to a unitary transform $\mathcal{U}_{\mathcal{N}} : AE \rightarrow BE$ when E is included. We denote the purification before channel as

$$\xi = \xi_{MAA'RE} = \Phi_{\Xi} \otimes |0\rangle\langle 0|_E, \quad (\text{D16})$$

and the final purification after channel as $\eta = \eta_{MBA'RE} = \mathcal{U}_{\mathcal{N}}(\xi)$. Below we show that $I(M[J]; BA'|M[J^c])_{\omega}$ is upper bounded by the right-hand side of Eq. (4) of the main paper.

Equivalently, since the purification systems R, E are traced out at the end and make no difference, we evaluate $I(M[J]; BA'|M[J^c])_{\omega}$ over η

$$\begin{aligned} I(M[J]; BA'|M[J^c])_{\eta} &= I(M[J]; BA'M[J^c])_{\eta} \\ &= I(M[J]A'[J]; BA'[J^c]M[J^c])_{\eta} \\ &\quad - I(A'[J]; BA'[J^c]M[J^c])_{\eta} + I(M[J]; A'[J])_{\eta}. \end{aligned} \quad (\text{D17})$$

The first equality is due to the chain rule of quantum mutual information and the independency constraint of MAC $I(M[J^c]; M[J]) = 0$. The second equality is due to the chain rule of quantum mutual information. Let $M[J] = X$, $BA'[J^c]M[J^c] = Y$ and $A'[J] = Z$, we have $I(M[J]; BA'M[J^c])_{\eta} = I(X; YZ) = I(Y; X|Z) + I(X; Z) = I(XZ; Y) - I(Z; Y) + I(X; Z)$, which equals the second line term by term. Note that the encoding does not affect the entanglement assistance A' , thus

$$I(M[J]; A'[J])_{\eta} = 0, \quad (\text{D18})$$

and from the positivity of quantum mutual information

$$I(A'[J]; BA'[J^c]M[J^c])_{\eta} \geq 0, \quad (\text{D19})$$

we have

$$I(M[J]; BA'|M[J^c])_{\eta} \leq I(M[J]A'[J]; BA'[J^c]M[J^c])_{\eta}. \quad (\text{D20})$$

As EA is unlimited, there is always an expanded system $A'_{\text{ex}} = \otimes_{i=1}^s A'_{\text{ex},i}$ available that includes A'_i, R_i, M_i for each sender i . Adopting the expanded EA,

$$I(M[J]A'[J]; BA'[J^c]M[J^c])_{\eta} \leq I(A'_{\text{ex}}[J]; BA'_{\text{ex}}[J^c])_{\eta}, \quad (\text{D21})$$

since, as a result of strong subadditivity of the Von Neumann entropy, discarding systems never increases quantum information. Note that $I(A'_{\text{ex}}[J^c]; A'_{\text{ex}}[J]) = 0$, combining Eq. (D20) and the equation above, we obtain the outer bound

$$I(M[J]; BA'|M[J^c])_{\eta} \leq I(B; A'_{\text{ex}}[J]|A'_{\text{ex}}[J^c])_{\eta} \quad (\text{D22})$$

for some pure state η , which is a product between different senders. With the expanded entanglement assistance $A' \equiv A'_{\text{ex}}$, we arrive at the desired outer bound for any encoding Ξ

$$I(M[J]; BA'|M[J^c])_{\eta} \leq I(B; A'[J]|A'[J^c])_{\rho}, \quad (\text{D23})$$

evaluated on the channel output $\rho = \mathcal{N} \otimes \mathcal{I}(\phi)$ of some pure product state $\phi = \phi_{AA'}$ that purifies the reduced state Ξ_A .

Denote \mathcal{T}_{ϕ} as a family of encodings, of which the overall state after the encoding satisfies $\Phi_{\Xi_A} = \phi$. Substitute the repetitive n uses of some encoding from \mathcal{T}_{ϕ} for the input of $\{\omega^{(u)}\}_{u=1}^n$ in Ineq. (C17), the left hand sides of Ineqs. (D23) gives an outer bound for information rates of the repetitive encoding. Thus one-shot, one-encoding rates are outer bounded by the region $\tilde{\mathcal{C}}_E(\mathcal{N}, \phi)$

$$\sum_{i \in J} \tilde{R}_i \leq I(B; A'[J]|A'[J^c])_{\rho}. \quad (\text{D24})$$

Finally, taking the convex hull on both sides of Ineq. (D23) and combining it with Theorem 3, for any $(n, R_1, \dots, R_s, \epsilon)$ code we have

$$\sum_{i \in J} R_i \leq \sum_u p_u I(M[J]; BA'|M[J^c])_{\eta^{(u)}} \quad (\text{D25})$$

for some encoding set $\{p_{\mathbf{m}_k^{(u)}}, \sigma^{\mathbf{m}_k^{(u)}}\}$ that generates state set $\{\eta^{(u)}\}$ by plugging $\Xi = \sum \mathbf{m}_k^n p_{\mathbf{m}_k^n} \sigma_{\mathbf{m}_k^n} \otimes |\mathbf{m}_k^n\rangle\langle \mathbf{m}_k^n|$ in Eq. (D16), and thereby

$$\sum_{i \in J} R_i \leq \sum_u p_u I(B; A'[J]|A'[J^c])_{\rho^{(u)}} \quad (\text{D26})$$

for some pure state sets $\{\phi^{(u)} = \Phi_{\Xi_{A^{(u)}}}\}$ that generate state sets $\{\rho^{(u)}\}$ by $\rho^{(u)} = \mathcal{N} \otimes \mathcal{I}(\phi^{(u)})$, with $\{p_u\}$ satisfying $\sum_u p_u = 1$. Thus the convex hull $\mathcal{C}_E^{(1)}(\mathcal{N})$ provides an outer bound for the $(n, R_1, \dots, R_s, \epsilon)$ code rate

$$\mathcal{C}_E^{(1)}(\mathcal{N}) \subseteq \text{Conv} \left[\bigcup_{\phi} \tilde{\mathcal{C}}_E(\mathcal{N}, \phi) \right]. \quad (\text{D27})$$